ADVANCED MATERIALS TECHNOLOGIES
www.advmattechnol.de

# Synergistic Integration of Hydrogen Peroxide Powered Valveless Micropumps and Membraneless Fuel Cells: A Comprehensive Review

*Jawayria Mujtaba, Aleksei Kuzin, Guoxiang Chen, Fenyang Zhu, Fedor S. Fedorov, Brij Mohan, Gaoshan Huang,* Valeri Tolstoy, Vadim Kovalyuk, Gregory N. Goltsman, Dmitry A. Gorin, Albert G. Nasibulin, Shuangliang Zhao, Alexander A. Solovev,* and Yongfeng Mei*

**Catalytic valveless micropumps, and membraneless fuel cells are the class of devices that utilize the decomposition of hydrogen peroxide ($H_2O_2$) into water and oxygen. Nonetheless, a significant obstacle that endures within the discipline pertains to the pragmatic open circuit potential (OCP) of hydrogen peroxide FCs ($H_2O_2$ FCs), which fails to meet the theoretical OCP. Additionally, bubble formation significantly contributes to this disparity, as it disrupts the electrolyte's uniformity and interferes with reaction dynamics. In addition, issues such as catalyst degradation and poor kinetics can impact the overall cell efficiency. The development of high-performance $H_2O_2$-FCs necessitates the incorporation of selective electrocatalysts with a high surface area. However, porous micro-structures of the electrode impedes the transport of fuel and the removal of reaction byproducts, thereby hindering the attainment of technologically significant rates. To address these challenges, including bubble formation, the review highlights the potential of integrating electrokinetic and bubble-driven micropumps. An alternative approach involves the spatiotemporal separation of fuel and oxidizer through the use of laminar flow-based fuel cell (LFFC). The present review addresses multifaceted challenges of $H_2O_2$-powered FCs, and proposes integration of electrokinetic and bubble-driven micropumps, emphasizing the critical role of bubble management in improving H2O2 FC performance.**

## 1. Introduction

The necessity for clean energy sources has become urgent given by humanity's attempts to decrease the use of fossil fuels, diminish the world's carbon footprint, address issues of global warming, energy gap, and dramatic air pollution. Although hydrogen fuel is a promising alternative, high operation pressure, storage difficulty, flammability, and absence of gaseous fuel infrastructure has prohibited any wide-scale industrial use. $H_2O_2$ is a high energy-density fuel (aqueous 60% $H_2O_2$: 3.0 MJ $l^{-1}$ or 2.1 MJ $kg^{-1}$) comparable to hydrogen (2.8 MJ $l^{-1}$, 3.5 MJ $kg^{-1}$ at 35 MPa).[1] Recent advancements in the production of $H_2O_2$ via the utilization of sunlight, water, and atmospheric oxygen have led to the recognition of $H_2O_2$ as a promising liquid solar fuel.[2]

$H_2O_2$ FCs boast several advantages over traditional hydrogen-oxygen fuel cells ($H_2$-$O_2$ FCs). First, $H_2O_2$ possesses

J. Mujtaba, G. Chen, F. Zhu, G. Huang, A. A. Solovev, Y. Mei
Department of Materials Science
Fudan University
Shanghai 200433, P.R. China
E-mail: gshuang@fudan.edu.cn; Solovev@fudan.edu.cn

A. Kuzin, V. Kovalyuk, G. N. Goltsman
National Research University Higher School of Economics
Moscow 101000, Russia

A. Kuzin, F. S. Fedorov, D. A. Gorin, A. G. Nasibulin
Center for Photonic Science and Engineering
Skolkovo Institute of Science and Technology
3 Nobel Str, Moscow 121205, Russia

The ORCID identification number(s) for the author(s) of this article can be found under https://doi.org/10.1002/admt.202302052

DOI: 10.1002/admt.202302052

B. Mohan
Centro de Quimica Estrutural, Institute of Molecular Sciences
Instituto Superior Tecnico
Universidade de Lisboa
Av. Rovisco Pais, Lisboa 1049-001, Portugal

V. Tolstoy
Saint Petersburg State University
Institute of Chemistry
26 Universitetskii Prospect, Petergof, St. Petersburg 198504, Russia

V. Kovalyuk
Laboratory of Photonic Gas Sensors
University of Science and Technology MISIS
Moscow 119049, Russia

G. N. Goltsman
Quantum Photonic Integrated Circuits Group
Russian Quantum Center
Skolkovo 143025, Russia

 

a higher energy density than liquid hydrogen, enabling $H_2O_2$ FCs to deliver more energy per unit volume. Additionally, the storage and transportation of $H_2O_2$ are simpler compared to hydrogen gas, which requires high-pressure or cryogenic conditions. The emergence of liquid $H_2O_2$ FCs has brought focus to the potential of $H_2O_2$ as a fuel and oxidizer, thereby facilitating the development of more environmentally friendly energy conversion technologies. Also, it poses lower explosion risks and is easier to handle. In FCs, $H_2O_2$ functions as both fuel and oxidizer in membraneless, one compartment, one reactant, and mixed reactant configurations.[3,4] $H_2O_2$ acts simultaneously as fuel and oxidizer and decomposes into environmentally friendly products: pure oxygen and water. Membraneless one-compartment $H_2O_2$ FCs configuration offers simplicity and a cost-efficient advantage due to a lack of an electrolytic membrane (e.g., Nafion). While cost considerations vary, $H_2O_2$ FCs show promise in becoming cost-competitive with conventional alternatives, especially when considering factors such as storage, transportation, and safety. Moreover, the potential for higher purity in $H_2O_2$ synthesis ensures consistent fuel cell performance. Simpler fuel cell designs are achievable with $H_2O_2$ FCs, as they eliminate the need for a separate oxygen supply system. Furthermore, efficiency improvements may be realized due to the direct decomposition of hydrogen peroxide. Benefits of $H_2O_2$ in terms of energy density, safety, and stability, with a particular focus on the development of high-power-density FCs utilizing specific catalyst complexes are discussed.[5,6] Significant development in the field is the shift toward using liquid fuels, such as $H_2O_2$ and sodium borohydride ($NaBH_4$). FCs' that employ these liquids have achieved a voltage output that surpasses conventional $H_2O_2$ FCs by over 30 percent.[7]

Today, one major challenge in the field – the practical OCP of the presented FCs is lower than the theoretical OCP value (1.09 V).[8] The potential solution consists of the discovery of a more selective electrocatalytic anode and cathode toward $H_2O_2$ electrooxidation and electroreduction,[9] separation of fuel-oxidant using laminar co-flows,[10,11] introduction of redox couples[12,13] and an application of high-surface area electrodes.[14] Recently, $H_2O_2$ FCs with 3D electrodes achieved a maximal areal power density of up to 300 W $m^{-2}$.[15] The power density of kW $m^{-2}$ can be achieved by employing a mixed reactant approach.[16] The utilization of laminar flow-based fuel cells (LFFCs) provides spatiotemporal separation of fuel/oxidant by eliminating the necessity of an electrolytic membrane, such as using co-laminar flows. Nevertheless, the pumping of laminar fuels/oxidants both through micro-channels and 3D electrodes costs a significant amount of energy. The advancement of $H_2O_2$ FCs has encountered a hurdle in timely delivery of fuel/oxidant, and removal of reaction products that hold technological significance, resulting in a stagnation of progress.

Approximately two decades ago, independently from the $H_2O_2$ FCs research, a new class of peroxide-driven micro-devices emerged. Bimetallic catalytic nano- micro- motors[17] and autonomous pumps[18–20] powered by decomposition of $H_2O_2$ have been demonstrated. Self-powered electrokinetic micropumps have been successfully integrated into electrodes of thin film FCs by depositing catalysts on the opposite sides of a porous membrane.[21] However, bubbles nucleation/generation on the porous electrode limits applications of membraneless FCs at higher concentrations of $H_2O_2$. Using conical catalytic microtubes, optimal chemical conditions, highly efficient bubble-driven micropumps operating up to × 1000 lower concentration of $H_2O_2$ ($10^{-4}$% v/v) has been developed.[22] Subsequently, using optimal physicochemical properties: reaction-diffusion, surfactants, and architecture of individual catalytic micropump, a highly compact efficient micropump powered by the recoil of oxygen microbubbles has been demonstrated. Integrating catalytic nanopumps into $H_2O_2$ FCs could potentially address several challenges in various ways. First, autonomous delivery of fuels/oxidants: catalytic nanopumps move fluids at the microscale, enabling them to deliver the $H_2O_2$ fuel to the electrode surfaces. The efficiency of the FCs can be enhanced by ensuring a steady supply of fuel without requiring an external energy source or mechanical pump.[23] Second, the removal of reaction products: catalytic pumps can also help in the timely removal of gaseous reaction products like $O_2$, which can otherwise accumulate and block the electrodes, hampering the performance of FCs. Third, improvement of energy efficiency: by precisely controlling the supply of fuel and removal of reactions' products, catalytic pumps can improve power output characteristics of the FCs. Fourth, one-compartment structure: catalytic pumps can support the design of FCs with a one-compartment structure.[24] Without the need for a membrane to separate the anode and cathode compartments, the design and manufacturing process of the FCs can be simplified, reducing the cost and complexity.[25] Fifth, longevity and durability: by managing fuel delivery and reaction product removal, integrated micropumps can also extend the lifespan of the fuel cell, reducing wear of the electrodes.[26] Therefore, the integration of catalytic pumps could provide a promising approach to solve the current issues facing membraneless $H_2O_2$ FCs. Thus, hydrogen peroxide fuel cells possess unique advantages over other fuel cell types, particularly in specific scenarios. For example, hydrogen peroxide fuel cells can be used in applications prioritizing safety, space-constrained environments, remote or off-grid power generation, areas with limited access to

S. Zhao
Guangxi Key Laboratory of Petrochemical Resources Processing and Process Intensification Technology and School of Chemistry and Chemical Engineering
Guangxi University
Nanning 530004, P. R. China
Y. Mei
Department of Materials Science & State Key Laboratory of Molecular Engineering of Polymers
Fudan University
Shanghai 200433, P. R. China
Y. Mei
International Institute of Intelligent Nanorobots and Nanosystems
Fudan University
Shanghai 200433, P. R. China
Y. Mei
Shanghai Frontiers Science Research Base of Intelligent Optoelectronics and Perception
Fudan University
Shanghai 200433, P. R. China
Y. Mei
Yiwu Research Institute of Fudan University
Yiwu, Zhejiang 322000, P. R. China

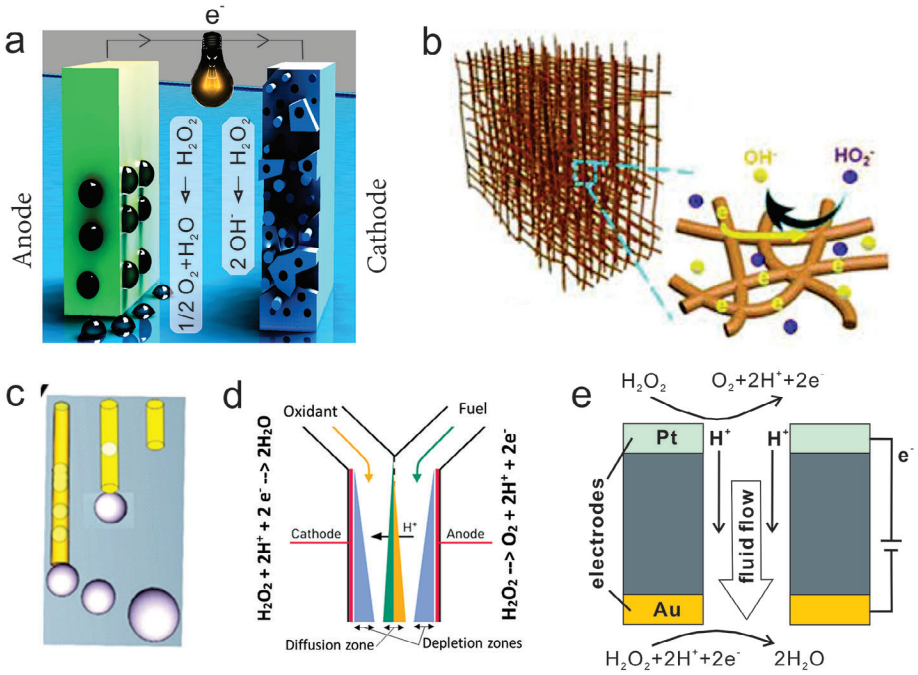


**Figure 1.** Examples of membraneless and microfluidic $H_2O_2$-FCs architectures and different flow configurations. a) Schematic image of one-compartment $H_2O_2$ FC consisting of two electrodes immersed in an $H_2O_2$ solution. b) Schematic image of high surface area porous electrode based on a silver-wire aerogel. Reproduced with permission.[15] Copyright 2019, Royal Society of Chemistry. c) Schematic image of catalytic tubular micropumps with different lengths generating bubbles during decomposition of peroxide. d) The concept of LFFC, where oxidant and fuel are spatio-temporally separated in the microchannel with depletion and diffusion zones. Adapted with permission.[30] Copyright 2004, Elsevier. e) Membraneless $H_2O_2$ FC with self-powered electrokinetic micropump. Adapted with permission.[21] Copyright 2010, John Wiley and Sons.

traditional fuel sources, varied operating conditions, and situations requiring reduced infrastructure requirements.[11,27,28] It can be achieved due to due to their superior safety, higher energy density, simplified design, renewable feedstock versatility, operational flexibility, and reduced infrastructure requirements, making them ideal for applications prioritizing safety, space efficiency, simplicity, sustainability, and operational adaptability.

A major thrust of this review examines state-of-the-art advancements in $H_2O_2$ FCs, including discussions about highly selective electrocatalytic anodes and cathodes specific to $H_2O_2$ electrooxidation and electroreduction, utilizing laminar co-flows to separate fuel-oxidant, incorporating redox couples, deploying high-surface area electrodes and the exploration of the potential benefits of integrating autonomous catalytic micropumps into $H_2O_2$ FCs. Three principal segments are discussed: a) an intricate discussion on the design methodologies and the implementation of autonomous catalytic micropumps, b) rigorous scrutiny of how the chemical characteristics of the fuel/oxidant contribute to the performance dynamics of $H_2O_2$ FCs, and c) an exhaustive survey of the most recent advancements in selective electrocatalysts, which are poised to significantly augment the efficiency and longevity of $H_2O_2$ FCs. The culmination of this review suggests that the persistent efforts in the development and refinement of high-performance $H_2O_2$ FCs could potentially instigate a revolutionary shift in the realm of sustainable energy research, thereby unlocking novel avenues for exploration and technological advancement. **Figure 1** displays a variety of designs and flow configurations for membraneless and microfluidic FCs. Figure 1a shows a one-compartment $H_2O_2$ FC with two electrodes immersed in an $H_2O_2$ solution. Figure 1b depicts a high surface area electrode constructed from a silver-wire aerogel.[15] Figure 1c illustrates catalytic tubular micropumps of varying lengths that produce bubbles during peroxide decomposition. Figure 1d presents the LFFC concept, where oxidant and fuel are spatially and temporally separated in the microchannel citechoban2004microfluidic. Figure 1e portrays a membraneless $H_2O_2$ FC with a self-powered electrokinetic micropump.[21] The research concept of $H_2O_2$-FCs can be integrated with the core technologies of catalytic nano-/micro-motors and pumps, developed in the past decade.[22,29,30] Optimizing FCs performance necessitates an interdisciplinary approach that integrates the engineering and synthesis of catalytic electrodes with autonomous micropumps for efficient mass transport, a comprehensive physicochemical analysis of the fuel and oxidant to understand their impact on electrochemical kinetics, and extensive characterization of highly-selective electrocatalysts to evaluate their electrocatalytic activity, selectivity, and stability under operational conditions.

## 2. Reaction Kinetics of $H_2O_2$ Decomposition

The decomposition of $H_2O_2$ serves as a case study in chemical kinetics. The thermodynamics of this reaction reveal it to be exothermic. From a kinetic perspective, the rate of this decomposition can be markedly accelerated in the presence of specific catalysts. Notably, certain transition metals and enzymatic

compounds have been empirically demonstrated to enhance the rate of $H_2O_2$ decomposition by lowering the activation energy barrier, thereby providing a mechanistic pathway for accelerated reaction rates. The rate of $H_2O_2$ decomposition is influenced by factors such as pH, temperature, and $H_2O_2$ concentration. In acidic conditions, the decomposition is stabilized, while in alkaline conditions, the rate can increase. The kinetics of this reaction provide insights into the mechanisms and pathways through which $H_2O_2$ breaks down, typically yielding water and oxygen. Understanding these kinetics is crucial for applications where controlled release of oxygen is desired or where the stability of $H_2O_2$ is of concern. Acidic media is preferred for stabilizing $H_2O_2$. Reaction kinetics of $H_2O_2$ decomposition can be studied via in situ visualization of oxygen evolution, combined with bright-field microscopy and high-performance liquid chromatography. For example, the rate of $H_2O_2$ decomposition can be evaluated using measurements of the diameter of $O_2$ bubbles in time. Reaction kinetics of the $H_2O_2$ decomposition can be studied in solutions with different pH.[31] Under OCP the net current is zero and the overall reaction takes place: $H_2O_2 \rightarrow O_2 + H_2O$. Mechanisms of $H_2O_2$ decomposition in chemical/electrochemical, in acidic and alkaline solutions are different. It is known that at lower pH values, the $H_2O_2$ reacts with $H^+$ to form the oxonium ion: $H_2O_2 + H^+ \rightarrow H_3O_2^+$ that reduces the initial $H_2O_2$ decomposition due to high content of $H^+$ ions. Simultaneously, the OH* can be scavenged by excess $H^+$: $OH^* + H^+ + e^- \rightarrow H_2O$, impeding the oxidation of $H_2O_2$: $H_2O_2 + OH^* \rightarrow HOO^* + H_2O$. Subsequently, due to two possible reactions highly acidic conditions reduce the decomposition of $H_2O_2$. At the same time, high pH values reduce the reaction rate due to the reaction between OH* and $HO_2^-$: $OH^* + HO_2^- \rightarrow O_2^+ + H_2O$ that is unfavourable side reaction of the equation: $H_2O_2 + OH^* \rightarrow HOO^* + H_2O$. OH* has a higher reaction rate with $HO_2^-$ than with $H_2O_2$ in acidic solutions, decreasing the decomposition of $H_2O_2$. A combination of above-mentioned effects leads to a maximum reaction rate at pH = 4. Kinetic models will be developed to identify the reaction rate constant and activation energy of peroxide decomposition reaction (depending on $H_2O_2$ feeding rate, temperature, pH). The reaction density functional theory (DFT) calculations will be performed and compared to experimental results. In acid media: $H_2O_2$ reduction reaction (HPRR) takes place: $H_2O_2 + 2H^+ + 2e^- \rightarrow 2H_2O$ ($E^0 = 1.78$ V vs. SHE). Due to a high potential $H_2O_2$ oxidation reaction can take place (HPOR): $H_2O_2 \rightarrow O_2 + 2H^+ + 2e^-$ ($E_a^0 = 0.69$ vs. SHE, where $E_a^0$ is the standard electrode potential of the HPOR). In addition, since $O_2$ is generated, the $O_2$ reduction reaction (ORR) occurs: $O_2 + 4H^+ + 4e^- \rightarrow 2H_2O$ ($E_c^0 = 1.23$ vs. SHE, where $E_c^0$ is the standard electrode potential of the ORR.[3] In alkaline media: $H_2O_2$ can be in the form of $HO_2^-$ due to reaction: $H_2O_2 + OH^- \rightarrow HO_2^- + H_2O$. Hydroxyl ions are formed in the reaction with $H_2O$: $HO_2^- + H_2O + 2e^- \rightarrow 3OH^-$ ($E_c^0 = 0.87$ V vs. SHE). Likewise, the HPOR can occur in alkaline conditions: $HO_2^- + OH^- \rightarrow O_2 + H_2O + 2e^-$ ($E_a^0 = 0.15$ V vs. SHE). Moreover, ORR can occur: $O_2 + 2H_2O + 4e^- \rightarrow 4OH^-$ ($E_c^0 = 0.4$ V vs. SHE).

## 3. Application of $H_2O_2$ as a Fuel and Oxidant, in Alkaline and Acidic Media

$H_2O_2$ has emerged as a pivotal compound in advanced electrochemical systems due to its dual functionality as both a fuel and an oxidant. In acidic media, $H_2O_2$ undergoes a reduction reaction, leading to the formation of water, while concurrently releasing electrons that can be harnessed for electrical work. Conversely, in alkaline environments, $H_2O_2$ can act as an effective oxidant, facilitating the electrochemical generation of molecular oxygen. The redox behavior of $H_2O_2$ is profoundly influenced by the pH of the medium, which dictates its electrochemical pathways and thermodynamic potentials. This pH-dependent versatility of $H_2O_2$ not only broadens its applicability across various electrochemical devices but also offers opportunities for optimizing energy conversion efficiencies. The integration of $H_2O_2$ in both acidic and alkaline systems underscores its potential as a sustainable and efficient electrochemical agent in next-generation energy technologies. Since HPRR can occur both in acid $H_2O_2 + 2H^+ + 2e^- \rightarrow 2H_2O$ ($E_c^0 = 1.78$ V vs. SHE) and alkaline media ($HO_2^- + H_2O + 2e^- \rightarrow 3OH^-$ ($E_c^0 = 0.87$ V vs. SHE)) $H_2O_2$ can be used as a fuel and oxidizer, respectively. $H_2O_2$ as an oxidant (in acid media) has a high potential (1.78 V). It is known that direct acidification of $H_2O_2$ leads to an enhancement of $H_2O_2$ electroreduction. To achieve high FCs performance $H_2O_2$ as an oxidant can be combined with many other fuels (e.g., borohydride, ethanol, hydrazine, formic acid, metals). This type of FCs typically combines $H_2O_2$ oxidant with alkali (KOH, NaOH), borohydrides, ethanol, metals as the fuel.[3] $H_2O_2$ can be used as a fuel due to its property to donate electrons in the oxidation reaction. A combination of reaction $HO_2^- + OH^- \rightarrow O_2 + H_2O + 2e^-$ ($E_a^0 = 0.15$ V vs. SHE) at the anode and $H_2O_2 + 2H^+ + 2e^- \rightarrow 2H_2O$ ($E_c^0 = 1.78$ V vs. SHE) at the cathode can be used to set the thermodynamic potential difference of FC. In detail, it can be accomplished using alkali added to the anolyte and acid to the catholyte. In principle, direct peroxide/peroxide FCs' operate with acidified $H_2O_2$ (e.g., adding $H_2SO_4$) as an oxidant and alkalized $H_2O_2$ (e.g., adding NaOH) as a fuel. Active electrocatalysts highly selective toward $H_2O_2$ electrooxidation in alkaline media and $H_2O_2$ electroreduction in acidic media are of high interest to develop. In $H_2O_2$ FCs half-reactions proceed on an anode and cathode, respectively. Reactions taking place at the cathode: $H_2O_2 + 2H^+ + 2e^- \rightarrow 2H_2O$ (1.78 V vs. NHE = normal hydrogen electrode, at the anode: $H_2O_2 \rightarrow O_2 + 2H^+ + 2e^-$ (0.68 V vs. NHE) and in total: $2H_2O_2 \rightarrow 2H_2O + O_2$ (1.09 V). $H_2O_2$ do not only accept electrons in the reduction reaction, but it can also donate electrons in the oxidation reaction.[4] This unique characteristic drives to use hydrogen peroxide simultaneously as an electron acceptor (oxidant) and an electron donor (fuel). Since $H_2O_2$ reduction reaction can take place in both acidic and alkaline media, as such, $H_2O_2$ is extensively used in acid-type, alkaline-type, and hybrid-type FCs. However, the $H_2O_2$ in acid media is preferred primarily due to enhanced electroreduction and its intrinsically high potential (1.78 V).

## 4. Synthesis of Hydrogen Peroxide

$H_2O_2$ is importance chemical product and that is identified as a "green" oxidant. Because of the sole produces $H_2O$ and $O_2$ when it decomposes, $H_2O_2$ is widely used in various fields, such as paper and textile manufacturing and environmental protection for detoxification and the decolorization of waste dye. So far, it is known that industrialized $H_2O_2$ production almost relies on the anthraquinone oxidation (AO) process, which is an

energy-intensive processes, and that oxidation process is obviously environmentally hazardous.[32] Generally, the $H_2O_2$ production process is as follows.[33–35] First of all, pure $H_2$ is indispensable to hydrogenation, which is mainly obtained by steam reforming. Second, the reactant of quinone needs to execute the hydrogenation process over the functional Pd-based catalysts. Third, the hydrogenated quinone should be filtered and then oxidized with air to form $H_2O_2$. However, a high concentration of $H_2O_2$ produced by the AO process adds additional challenges due to safety concerns. Hence, it is necessary to develop an energy efficient and green alternative $H_2O_2$ production technique.

Over the past few decades, the direct synthesis of hydrogen peroxide (DSHP) from molecular hydrogen and oxygen has become the alternative technique for $H_2O_2$ production.[36–39] Compared with the complicated AO process, the DSHP progress only requires the reactants of $O_2$ and $H_2$ on the surface of catalyst, on which the $H_2$ occurs dissociative adsorption and subsequently to participate in hydrogenation process to form $H_2O_2$. The DSHP process can be a more suitable solution to small-scale facilities with low concentration of $H_2O_2$, and the only byproduct is water. It can improve safety by avoiding the transportation of highly concentrated $H_2O_2$ solution. However, the DSHP process remains challenging where the key problem is stabilizing the resulting $H_2O_2$ so that it does not decompose and form water. And the side reaction to produce $H_2$ is more thermodynamically spontaneous during the production of $H_2O_2$.

Recently, the electrochemical two-electron oxygen reduction strategy offers an attractive route for on-site production of $H_2O_2$, as it could effectively resolve the issues associated with the AO process and DSHP process.[40,41] Indeed, the electrochemical oxygen reduction route through using only $O_2$, $H_2O$ and electricity as inputs with no waste released, which is safer, equally ecological and proceed under mild conditions such as ambient temperature and pressure. Moreover, the oxygen reduction reaction process can be coupled with renewable energy sources and thus can be used in remote regions.

Generally, the electrochemical reaction reactor for $H_2O_2$ production is mainly conducted by a traditional H-cell or flow cell types with gas diffusion layers.[42] It is well-known that limited mass-transport is a disadvantage of traditional H-cell. To solve the inherent deficiency, the alternative continuous flow cell has been introduced, and received more concern for electrochemical $H_2O_2$ production. Although electrochemical production of $H_2O_2$ is a viable alternative to the conventional AO, both the performance of catalysts and reactors should be improved in the future. Thus, we focus on the recent progress of catalysts and cells design for electrochemical $H_2O_2$ production. Recently, density functional theory (DFT) calculations provide a shortcut for screening high performance catalysts in various electrochemical reactions, including of hydrogen evolution reaction (HER), carbon dioxide reduction reaction ($CO_2$RR), nitrogen evolution reaction ($N_2$RR), ORR and so on.[43–45] Thus, in this review, it is worth first mentioning the current understanding of the two-electron or four-electron ORR mechanism. In the electrochemical processes, both the two-electron and four-electron ORR steps are illustrated as following:[40,46]

The two-electron pathway:

$$O_2 + 2(H^+ + e^-) \rightarrow H_2O_2 (E^o = 0.70V) \quad (1)$$

$$O_2 + 2(H^+ + e^-) \rightarrow {}^*OOH + (H^+ + e^-) \quad (2)$$

$${}^*OOH + (H^+ + e^-) \rightarrow H_2O_2 \quad (3)$$

The four-electron pathway:

$$O_2 + 4(H^+ + e^-) \rightarrow 2H_2O (E^o = 1.23V) \quad (4)$$

$$O_2 + 4(H^+ + e^-) \rightarrow {}^*OOH + 3(H^+ + e^-) \quad (5)$$

$${}^*OOH + 3(H^+ + e^-) \rightarrow {}^*O + 2(H^+ + e^-) + H_2O \quad (6)$$

$${}^*O + 2(H^+ + e^-) + H_2O \rightarrow {}^*OOH + (H^+ + e^-) + H_2O \quad (7)$$

$${}^*O + 2(H^+ + e^-) + H_2O \rightarrow {}^*OOH + (H^+ + e^-) + H_2O \quad (8)$$

It is clear that there are three different reaction intermediates (i.e., *OOH, *O, *OH) for four-electron pathway and the sole *OOH intermediate for two-electron pathway. Up to now, the computational hydrogen electrode (CHE) model has been proposed and developed by Norskov and his coworkers, which is the available method to analyze the ORR activity and selectivity.[44,47] In the CHE model, the free energy of a single proton-electron pair ($H^+ + e^-$) is defined as -e$U$ relative to $H_2$ in the gas phase at standard conditions, where $U$ is the electrode potential (vs. RHE). To calculate the adsorption free energies and/or reaction free energies, the general equation can be defined by

$$\Delta G = \Delta E + \Delta ZPE - T\Delta S - neU \quad (9)$$

where the $\Delta E$, $\Delta$ZPE, T$\Delta S$, and $n$ are for the DFT calculated binding energy, zero-point energy, entropic corrections, and related electron number, respectively.

According to the advanced benchmark of CHE model for two-electron and/or four-electron ORR activity and selectivity, tremendous theoretical and experimental research progresses have been achieved to design high-performance catalysts.[34,48] Here, both the noble metal-based catalysts and single-atoms catalysts (SACs) are dominant taken into account. Noble metal-based catalysts have received much attention, such as Pd, Pt, and Ru, which is ascribed to the highly activity, selectivity, and stability (**Figure 2a**).[49,50] Especially, the two-electron ORR activity and selectivity on these noble metals can be further improved by alloying process with other metals, such as Au, Ag, Sn, Hg, and so on.[34,51–53] By means of DFT calculations, Jirkovský et al. proposed that isolated alloying atoms of Pd, Pt, or Rh placed within the Au surface should enhance the $H_2O_2$ production relative to pure Au.[54] Further, the experimental results exhibited that increasing the Pd concentration to 8% can obtain an ultrahigh $H_2O_2$ selectivity of 95%. However, increasing of Pd concentration (≈ 50%) in the PdAu alloy leads to an unremarkable $H_2O_2$ selectivity of 10% (Figure 2b). Siahrsotami et al. found that the Pt-Hg/C alloy exhibits an outstanding $H_2O_2$ selectivity of up to 96% and mass activity of ≈26 A $g^{-1}$ of noble metal at 50 mV overpotential (Figure 2c). The DFT calculations revealed that the $PtHg_4$ alloy has a suitable adsorption free energy for the sole intermediate of *OOH species (Figure 2d). Obviously, the main purpose of alloying process is to modify the binding energies of the intermediate species, and the ideal *OOH adsorption free energy is ≈4.22 eV for $H_2O_2$ production. For the two-electron pathway, the

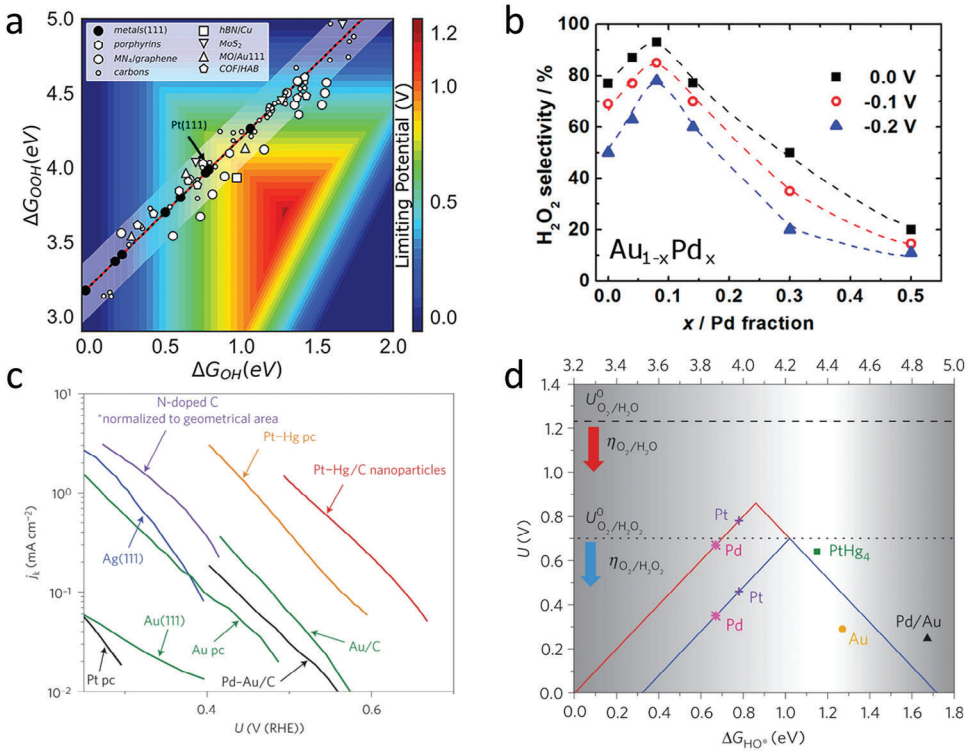


**Figure 2.** Theoretical and experimental results of metal-based catalysts for $H_2O_2$ production. a) 2-D volcano plot showing the scaling relationship between the adsorption free energies of *OOH and *OH for metal-based catalysts. Adapted with permission.[33] Copyright 2018, American Chemical Society. b) $H_2O_2$ selectivity as a function of palladium content. Adapted with permission.[55] Copyright 2011, American Chemical Society. c) the kinetic current as a function of potential with respect to reversible hydrogen electrode (vs RHE). Adapted with permission.[56] Copyright 2013, Nature Publishing Group. d) limiting potential (UL) as a function of the adsorption free energies of *OH (lower horizontal axis) and *OOH (upper horizontal axis). Adapted with permission.[57] Copyright 2020, Royal Society of Chemistry.

catalysts that bind *OOH strongly, *OOH→$H_2O_2$ is the potential limiting step, whereas for the weakly binding energy of *OOH, $O_2$→*OOH, is a potential limiting step. Developing and designing the catalysts that bind *OOH neither too strong nor too weak is a correct choice.

## 5. Single-Atom Catalysis of $H_2O_2$

SACs have attracted considerable attention in various electrochemical energy conversion processes, such as $CO_2$RR, $N_2$RR, HER, and ORR.[58,59] The specific reaction sites in the surface of SACs lead to an ultrahigh product selectivity for target reaction process. For example, the metal-nitrogen-doped carbons (M-N-Cs) as a unique class of SACs have explicit active sites (i.e., central metals, coordination atoms, surrounding carbon matrix) for various catalytic reactions (**Figure 3a**).[59]

Tang et al. reported that both the first and second coordination spheres (CSs) and central metals synergistically determines the electrocatalytic response for $H_2O_2$ production (Figure 3b). And the two-electron pathway can be preferred with the first (N or/and O coordination) and second (C-O-C groups) CSs.[60] Jung et al. found that the $H_2O_2$ activity on Co-$N_4$ moiety can be tailored by fine-tuning its surrounding atomic configuration with a specific epoxy group (Co-$N_4$(O) (Figure 3c).[42] The experimental results demonstrated that the Co-$N_4$ moiety modified by epoxy group exhibits an outstanding performance for $H_2O_2$ production, with a kinetic current density of 2.8 mA $cm^{-2}$ (at 0.65 V vs RHE) and a mass activity of 155 A $g^{-1}$. To simultaneously tune the coordination number of the Co-N-C moiety and the surrounding epoxy groups, a one-step microwave thermal shock has been adopted by Gong et al. In the 0.1M KOH, the synthesized low-coordinated Co-$N_2$ configuration and its surrounding abundant epoxide groups exhibit a high $H_2O_2$ selectivity (91.3%) and mass activity (44.4 A $g^{-1}$ at 0.65 V vs RHE) (Figure 3d).[61]

## 6. Design of the Electrochemical Reactors for $H_2O_2$ Production and Electrode Engineering Methods for Effective $O_2$ Bubble Transport

To date, the electrochemical reactors for $H_2O_2$ production can be divided into three types, including of H-cell, flow-cell, and microfluidic cell.[62] Usually, the rotating ring-disk electrode (RRDE) has been introduced as an working electrode of the classical H-cell to analyze the $H_2O_2$ selectivity and activity (**Figure 4a**). Typically, the glassy carbon disk part of working electrode is the provenance of $H_2O_2$, and the $H_2O_2$ oxidation occurs on the Pt ring electrode. And the Pt ring electrode has been held at 1.20 V (vs RHE) to quantify the $H_2O_2$ yield on the disk electrode. Additionally, the ring collection efficiency of RRDE can be determined by using a typical redox system of potassium ferricyanide solution. Thus, the $H_2O_2$ selectivity can be defined from the following formulas

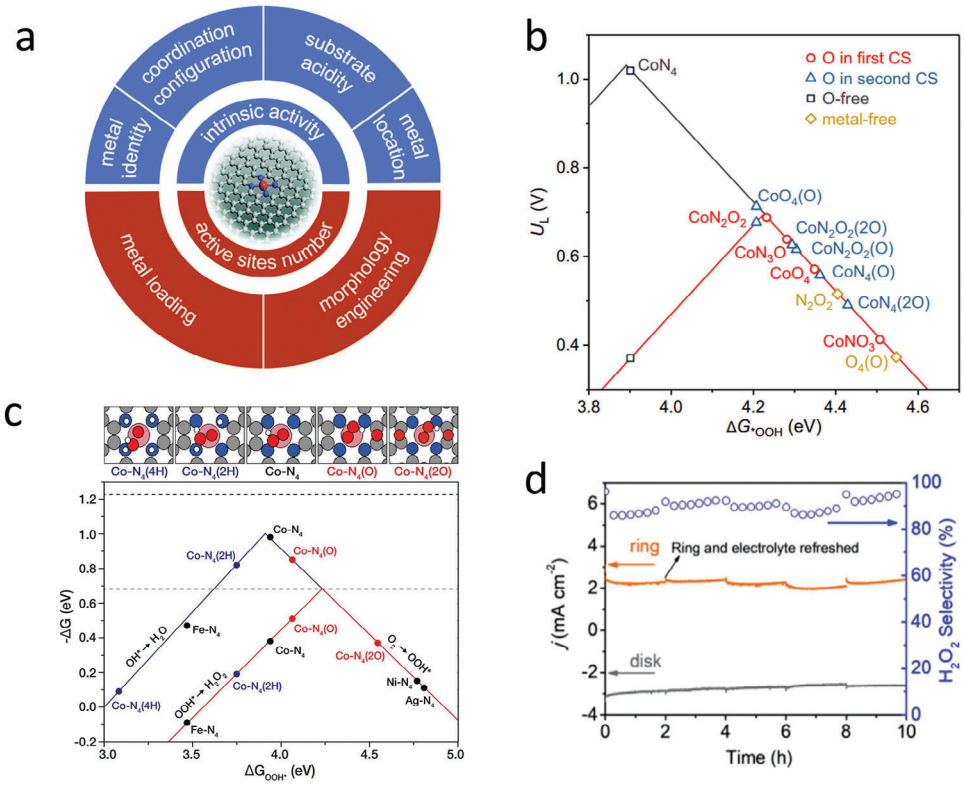


**Figure 3.** Single atom catalysts (SACs) for $H_2O_2$ production. a) Summarized the influence factors for the intrinsic activity and active sites number in SACs. Reproduced with permission.[59] Copyright 2019, American Chemical Society. b) Limiting potential volcano plots of ORR via the two-electron and four-electron pathway for SACs. Reproduced with permission.[60] Copyright 2021, American Chemical Society. c) Theoretical catalytic activity volcanoes for the $H_2O_2$ and $H_2O$ production. Reproduced with permission.[42] Copyright 2020, Springer Nature. d) Chronoamperometry stability test of Co-$N_2$-C/HO at 0.09 V in 0.1 M KOH. The inset plots the mass activity for SACs. Reproduced with permission.[61] Copyright 2022, John Wiley and Sons.

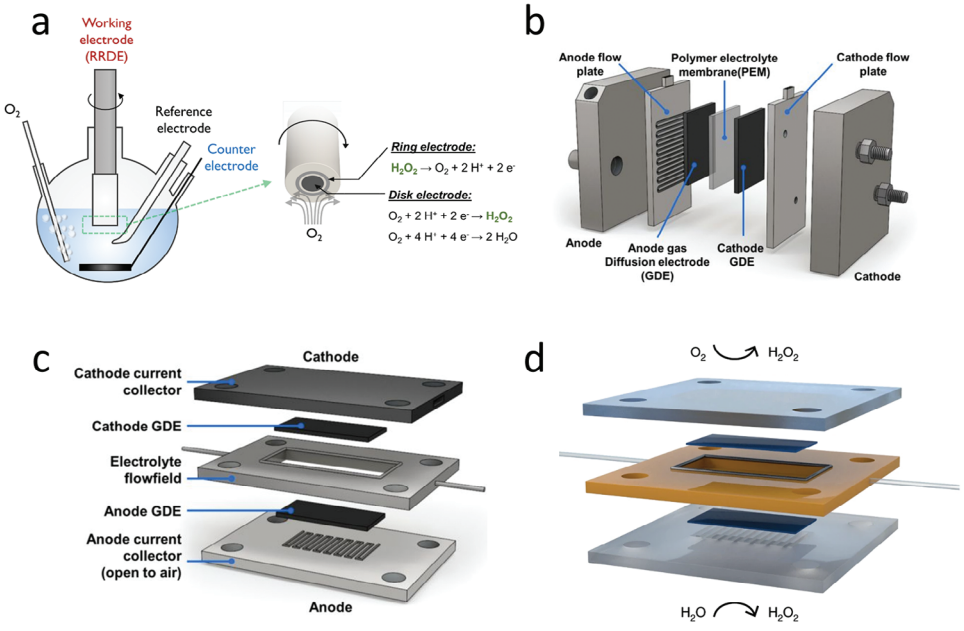


**Figure 4.** Electrochemical reactors for $H_2O_2$ production. a) A RRDE setup in a three-electrode electrochemical cell. Reproduced with permission.[64] Copyright 2018, American Chemical Society. b) Membrane-based flow reactor consisting of the anode and cathode on either side of a polymer electrolyte membrane. Reproduced with permission.[62] Copyright 2020, American Chemical Society. c) Microfluidic reactor consisting of a liquid electrolyte flow channel between the anode and cathode gas diffusion electrode materials. Reproduced with permission.[62] Copyright 2020, American Chemical Society. d) Schematic design of microfluidic reactor for $H_2O_2$ production. Reproduced with permission.[65] Copyright 2020, Springer Nature.

based on the collection efficiency of RRDE ($N$), the ring current ($I_r$) and disk current ($I_d$):[63]

$$\text{Selectivity}(\%) = 200 \times \left(\frac{I_r}{N}\right) / \left(\frac{I_r}{N} + I_d\right) \quad (10)$$

And the number of electrons transferred:

$$n = 4 \times I_d / \left(I_d + \frac{I_r}{N}\right) \quad (11)$$

According to Kouteský-Levich equation, the kinetic activity and mass transport of reactants can be analyzed:

$$\frac{1}{j_m} = \frac{1}{j_l} + \frac{1}{j_k} \quad (12)$$

where the kinetic current density, total current density, and the diffusion-limited current density are for the $j_m$, $j_l$, and $j_k$, respectively. The $H_2O_2$ concentration can be quantified by cerium sulfate ($Ce(SO_4)_2$) titration method:

$$M(H_2O_2) = 2 \times M(Ce^{4+}) \quad (13)$$

where the $M(Ce^{4+})$ represents the mole of consumed $Ce^{4+}$. To overcome the mass transport limitation of $O_2$ gas in the H-cell, the gas-diffusion electrodes (GDEs) have been adopted in recently studies (Figure 4b).[62,66,67] Normally, the GDEs are mainly composed of a porous material with a hydrophobic component, which can be regarded as a membrane between $O_2$ gas and the cathode electrolyte. To maintain the stabilized flow or transport of $O_2$ to the catalyst, the target catalyst can be coated onto the gas diffusion layer at the solid–liquid interface. The traditional slow diffusion process of $O_2$ in the liquid electrolyte can be avoided by the gas diffusion layer.

Since the advent of LFFCs in 2002, a great deal of research has focused on the cell designs for electrochemical energy conversion.[68] Ferrigno et al. first reported a pioneering single channel of redox fuel cell, the workable plan could be ascribed to the laminar flow effect (occurs in liquids flowing at low Reynolds number) that effectively eliminate convective mixing of fuels. Subsequently, Jayashree et al. proposed an air-breathing LFFC for oxygen reduction reaction.[69] By means of a gas diffusion electrode as the cathode, the LFFC exhibits a remarkable power density of 26 mW $cm^{-2}$. The advanced microfluidic cell also performed in electrochemical $H_2O_2$ production(Figure 4c).[62,67] Xia et al. recent research proposed a microfluidic cell for $H_2O_2$ production, where $H_2O_2$ can be generated on both the cathode and anode electrodes (Figure 4d).[65] On the one hand, the two-electron ORR occurs at the cathode. At the same time, the two-electron water oxidation process occurs at the anode. The experimental results demonstrated that this system achieved an ultrahigh $H_2O_2$ production rate of ≈ 24 μmol × $min^{-1}$.

Besides the cell design, electrode engineering methods optimized for oxygen bubble transport can play a pivotal role in improving the efficiency and performance of $H_2O_2$ FCs. Previous studies have highlighted the importance of catalyst layer (CL) design in determining catalyst utilization and, consequently, the efficiency of proton exchange membrane water electrolyzers (PEMWEs). Utilizing a four-phase stochastic reconstruction method, researchers have identified optimal values for parameters such as porosity, carbon agglomerate dispersion, ionomer content, and carbon support size within CLs.[70] Deviations from these optimal values result in transport issues for electrons, protons, and mass within CLs, ultimately limiting Pt utilization to around 50%. Addressing this challenge, a surfactant-assisted method has been proposed to manipulate nano/microbubbles generated during water electrolysis, thereby improving mass transfer rates and overall efficiency. Among the surfactants studied, potassium perfluorobutyl sulfonate (PPFBS) has shown significant promise due to its structural similarity to Nafion, resulting in decreased hygrogen evolution reaction overpotential and increased current density.[71] Furthermore, the development of 3D stack-printed catalysts, such as woodpile (WP)-structured Ir, has demonstrated marked improvements in ORR mass activity. By systematically controlling the 3D geometry, researchers have facilitated facile transport of evolved $O_2$ gas bubbles, leading to enhanced electrochemically active surface area (ECSA) and ECSA-specific activity.[72] These advancements underscore the importance of optimizing electrode engineering methods for efficient oxygen bubble transport in PEMWEs, paving the way for enhanced performance and scalability in electrolysis technologies. Thus, presented stochastic reconstruction method, three-dimensionally stack-printed catalysts and manipulating the generated nano/microbubbles using surfactants techniques can be adapted for improving LFFCs perfomance from point of oxygen bubble transport.

## 7. Materials Requirements for $H_2O_2$ FC

Selecting an appropriate electrode material necessitates a rigorous evaluation of its intrinsic and extrinsic properties. Foremost, its electrochemical activity should facilitate efficient electron transfer kinetics for the target redox reactions. The material's chemical stability under operational conditions is paramount to prevent deleterious corrosion or degradation phenomena. Electrical conductivity should be optimal, ensuring minimal resistive losses. A structured porosity is desirable, as it augments the electroactive surface area, thereby enhancing the electrode's electrocatalytic efficiency. Economic viability and material abundance are pivotal for scalable applications. In the sophisticated engineering of $H_2O_2$ FCs, the judicious selection of materials is paramount to ensure optimal electrochemical performance and robustness. The electrodes, pivotal in these cells, should not only catalyze the redox reactions of $H_2O_2$ efficiently but also exhibit resilience against its potential oxidative effects. $H_2O_2$ FCs require a thorough investigation of electrode characteristics, encompassing several essential prerequisites. These include the need for a large surface area, optimized mixed potential, efficient electrocatalytic activity, and precise selectivity. For cathode, the following materials can be used: PEDOT, Ag/Ag–Pb alloy, Ag nanowires, FeIII(Pc)Cl, Pt/C, $PbSO_4$/C, Au, Au/C, Pt, Pd, Pd/Ir, Pt/C, Prussian blue-Pt, Pd-Ag, Pd-Ir. For anode, the following materials can be chosen: Ni, Ni/CF, Au, Au/C, AuZn/Z Pt, Pt/C Pd, PdNi/C, Ni, Zn, carbon nanotube (CNT)-supported Prussian Blue, Pt/Ru nanoparticles, Pd/Pt, $Ni(OH)_2$, $Ag_2O$.[4] The main obstacle that impedes the practical use of $H_2O_2$ FCs is the high overvoltage at the cathode. One of the ways to solve this issue is to apply specific electrocatalysts to the surface of such electrodes, which

reduces the overvoltage values.[73] For instance, a $Fe[Co(CN)_6]$ layer can be used as an electrocatalyst on the cathode and Ag-Pb alloys. Electrocatalysts based on metal oxides, hydroxides and peroxides, among them are NiOOH, $La_xNbO_y$, $CeO_{2+x}$, $AgMnO_2$, $Bi_xVO_4$, can be synthesized via the Successive Ionic Layer Deposition (SILD)[74] or Gas-Solution Interface Technique (GSIT).[75] Requirements for nanomaterials are earth abundant, low cost, non-toxic, chemically-stable, selective, high surface area, high porosity, support effective mass transport and desorption of reactants, intermediates and products, high catalytic reactions rates to enable the efficient generation, transport and utilization of electrons and protons. Various electrocatalysts can be applied in $H_2O_2$ FC, such as at the anode (Au, Pt, Pd, Pt/C, Zn, Ni/Pt-C, PtCu/C and so on) and at the cathode (Prussian blue, $PbSO_4$/C, Au, Pt, Ag, Pd–Ag, Pd, Pd-Ir, Pt/C, $PbSO_4$/C). It should be noted that FCs with enzyme-based catalysts have high selectivity. However, they do not make it possible to obtain the required power values due to the slow reaction kinetics.[76] The use of electrocatalysts based on inorganic compounds is promising in terms of achieving a relatively high power. Early work showed that Ag wire could be used for FC with alkaline electrolyte as an electrocatalyst for HPRR at the cathode, and Au, Ni, Pt, or Pd wire - for HPOR at the anode.[9] The electrocatalytic properties in HPRR of electrodes made of other noble metals have been studied in a number of works[77–81] In particular, using Pt as an example,[82] it was shown that the (111) faces of crystals have the highest activity.

Transition metal oxides have been chosen as HPRR electrocatalysts in alkaline media in a number of works. Among such oxides are $Co_3O_4$,[83] $Co_2O_4$,[84] $LaNiO_3$,[85] and $La_2CuO_4$.[86] The possibility to create an electrocatalyst for HPRR based on W-doped $MoS_2$ nanosheets is reported previously.[87] A number of works have been devoted to the study of the electrocatalytic properties of nitrogen doped graphene nanoflakes in neutral solution.[88,89] Analysis of the results of studies of the electrocatalytic properties of metal oxides, $MoS_2$ and graphene showed that $Co_3O_4$-based catalysts deposited on the surface of a porous layer of gold on a foam nickel exhibit the greatest activity.[90] The current density for HPRR was 286 mA/cm$^2$ for a 3 M KOH and 0.4 M $H_2O_2$ solution at an electrode potential of – 0.4 V versus Ag/AgCl. However, most oxides cannot be used in this area due to their high solubility. Therefore, these electrocatalysts primarily include noble metals and a number of complex compounds, for example, Prussian blue,[91] nickel ferric ferrocyanide,[92] copper hexacyanoferrate,[93] Co, Cu, and Cu bis-phenanthroline.[94] Studies have shown that cathodes with copper hexacyanoferrate electrocatalyst have maximum power densities. This value is equal to 8.3 mW cm$^{-2}$. High specific surface and the presence of special morphology are other important characteristics of electrocatalysts. Moreover, the morphology should ensure the possibility of $H_2O_2$ molecules entering the solution-electrode interface and removing the reaction products. It has been shown that porous films of Ni, Co, and Cu-M alloys (M = Fe, Co, Ni) obtained by electrolytic deposition exhibit high electrocatalytic activity in HPRR in an alkaline medium.[95] Moreover, the Cu-Fe alloy has the greatest activity. A specific current of more than 8 mA cm$^{-2}$ was obtained. A number of works have been devoted to the study of the electrocatalytic properties of porous Au films. Usually, such films are obtained by electrolytic deposition of Au with Ag or Sn alloys on the surface of metal electrodes, followed by dissolution of a less noble metal.[90] Moreover, the pore sizes significantly affect the electrocatalytic properties. For example, a porous gold film with an average pore size of 30 nm has the best properties in HPRR.[96] As noted above, a 3D aerogel made of silver nanowires with a diameter of 250 nm and a length of up to 40 microns was proposed to be used as a DHPFC cathode.[15] Anode electrocatalysts for HPOR have better performance and stability compared to cathode ones. Therefore, fewer works are devoted to their study. Metals such as Ni or Au are often used as anodes. In particular, Ni has the lowest decomposition rate of $H_2O_2$. However, it has an appreciable solubility in acidic environments, and this is essential when creating one-compartment FC. Other electrocatalysts for HPOR include nickel/nickel oxide embedded N-graphene[97] cobalt phthalocyanine,[98] hollow cobalt nitrogen doped carbon catalyst,[99] and platinum nano islands on Au(111).[100] It was shown that vitamin B12 can be used as an electrocatalyst for HPOR at physiological pH values.[101] For the anode, as well as for the cathode, it is important to have a special 3D morphology. For example, it was found that the maximum anode current in FC was achieved for electrodes formed by nano-needles of nickel on the surface of TiC rods.[102] In the realm of Direct Borohydride-$H_2O_2$ FCs (DBHPFC), research has highlighted the importance of anode conditions, such as the electrocatalyst and fuel concentration, in influencing the system's performance.[103] Specifically, the concentration of $NaBH_4$ was found to significantly impact the mass and decomposition reaction rate, providing insights into the optimization of conditions for enhanced performance. A notable study employed a unique anode composition of $M_m$(misch metal) $Ni_{3.6}Al_{0.4}Mn_{0.3}Co_{0.7}$ paired with a gold-coated stainless-steel gauze cathode, achieving a peak power-density of 50 mW cm$^{-2}$ at 1 V, a significant improvement over the 9 mW cm$^{-2}$ observed from a methanol-hydrogen peroxide fuel cell.[104] Another research introduced a calibrated numerical model for a hydrogen-peroxide direct-borohydride fuel cell ($H_2O_2$-DBFC), emphasizing the balance between thermodynamic efficiency and parasitic reaction rates, with the choice of Au for the anode and Pd:Ir for the cathode being pivotal.[105] Further advancements were seen in a DBFC using a Ni-Pt/C composite as the anode catalyst, which achieved a peak power density of 140 mW cm$^{-2}$ at 55 °C.[106] Studies explored diverse approaches, such as the use of carbon-supported Prussian Blue as a cathode catalyst, which showcased unique electron-transfer properties,[107] and a DBFC with a Pd/Ir catalyzed microfibrous carbon cathode that highlighted the synergistic effects of alloy catalysts.[108] Another significant advancement was the use of gold nanoparticles on reduced graphene oxide foam as an anode material for the DBHPFC, which showcased enhanced electrocatalytic properties due to the synergistic effects of gold and graphene.[109] The introduction of a DEFC with a unique design using PdNi/C as the anode catalyst and Pt/C as the cathode catalyst highlighted the importance of material selection in optimizing electrochemical reactions.[110] Another insightful study on direct borohydride/peroxide FCs brought to the fore the importance of bipolar plate materials, flow fields, and manifold design in determining fuel cell efficiency. A notable finding from this study was that using sintered graphite with serpentine flow fields led to the highest single-cell power density, reaching 93.3 mW cm$^{-2}$.[111]

Transitioning to catalyst alternatives, atomically dispersed transition metal with nitrogen-doped carbon (M-N-C) has emerged as a promising contender to platinum group metal (PGM) catalysts.[112] The identification of Fe-N-C and Co-N-C as potential hydrogen peroxide reduction reaction (PRR) catalysts in direct borohydride FCs (DBFCs) suggests a potential shift in the paradigm of catalyst selection, emphasizing the exploration of non-traditional materials. Further research on direct borohydride FCs (DBFC) under varying conditions revealed an optimal peak power density of 130 mW $cm^{-2}$. The study emphasized the importance of balancing conditions like membrane thickness, temperature, and reactant concentration for optimal power density.[113] The study compared various electrocatalysts in a hydrogen peroxide direct borohydride fuel cell ($H_2O_2$-DBFC). The combination of palladium (Pd) and iridium (Ir) catalysts on a carbon substrate for the Al/$H_2O_2$ semi-fuel cell emphasized the importance of bimetallic catalysts in efficient electron transfer.[15] The Al-air semi-fuel cell (SFC) system, which co-generates $H_2O_2$, demonstrated superior performance using gas-diffusion electrodes (GDE) Black Pearls 2000(BP 2000) with an anion-exchange membrane (AEM) and 6M KOH electrolyte, emphasizing the importance of the KOH electrolyte in efficient ion transport.[114]

A significant finding was that a graded catalyst, transitioning from Pd/C at the channel inlet to Pt/C at the outlet, delivered the best performance. This suggests that employing catalyst gradients could pave the way for more efficient FCs, especially for flow-type reactant systems.[115] Further, research on a formic acid/hydrogen peroxide (HCOOH/$H_2O_2$) fuel cell emphasized the superior formic acid oxidation reaction of the 20% Pt-10%Sn/C system.[116] Lastly, a study on an alkaline aluminium hydrogen peroxide semi-fuel cell demonstrated its capability to power the autonomous underwater vehicle for extended underwater surveys.[117] Briefly touching upon other notable studies, research on Pt-Cu bimetallic nanoparticles showcased the Pt50Cu50/C catalyst's superior catalytic activity in direct borohydride-$H_2O_2$ FCs (DBHFCs).[118] Another study highlighted the potential of a Mg-$_2O_2$ FC using a noble metal-free carbon-based cathode.[119]

The transformation of Pt into hollow nanospheres resulted in a power output of 54.5 mW $cm^{-2}$, emphasizing the potential of morphological alterations in enhancing catalyst performance.[120] The alloying of platinum with tin further augmented its electrocatalytic efficiency, achieving an impressive 91.5 mW $cm^{-2}$ at 25 °C.[121] Gold, another noble metal, when structured into hollow nanospheres, yielded a power output of 25.8 mW $cm^{-2}$, suggesting the versatility of noble metals in fuel cell applications.[122] The combination of platinum and iron showcased a robust 65 mW $cm^{-2}$ at 25 °C, highlighting the synergistic effects of bimetallic combinations.[123] Similarly, the Pd-Co alloy, which capitalized on the combined electrochemical properties of both metals, reached a commendable 66.84 mW $cm^{-2}$ at the same temperature.[124] The $Pt_{67}Co_{33}$/C variant of carbon-supported Pt-Co nanoparticles emerged as a frontrunner, achieving a significant power density of 79.7 mW $cm^{-2}$ at 25 °C.[125] This result underscores the importance of nanoparticle support and its influence on electrocatalytic activity. $Co_3O_4$ nanoparticles, with their meticulous average diameter of around 17 nm, showcased a promising electroreduction activity for $H_2O_2$, indicating the potential of oxide nanoparticles in fuel cell applications.[83] A comparative study emphasized platinum's inherent electrochemical superiority for peroxide decomposition over other materials.[126]

The introduction of a FC with a bipolar membrane, combined with the PtRu/C anode catalyst, achieved a power density of 45.6 mW $cm^{-2}$, highlighting the role of membrane selection in fuel cell efficiency.[127] Nanoporous gold (NPG), known for its high surface area and conductivity, demonstrated its capability in the oxygen reduction reaction, emphasizing the importance of mesoporous metals in electrocatalysis.[128] The exploration of plasma-treated non-precious catalysts, such as Fe and Co porphyrins and phthalocyanines, revealed their potential in rivaling the performance of noble metal-based catalysts, achieving 1.4 times their power.[129] One of the most notable findings is the use of dealloyed nanoporous gold leaves (NPGLs) as electrocatalysts in direct hydrazine-$H_2O_2$ FCs (DHHPFC). These NPGLs have demonstrated an open circuit voltage (OCV) of 1.2 V at 80 °C and a remarkable maximum power density of 195 mW $cm^{-2}$, which is a substantial 22-fold increase compared to traditional Pt/C electrocatalysts.[130]

Further emphasizing the role of material innovation, a study on direct peroxide-peroxide FCs showcased the superior catalytic performance of dendritic Pd electrodeposited on carbon fiber cloth (CFC) for both $H_2O_2$ electrooxidation in KOH solution and electroreduction in $H_2SO_4$ solution.[81] This electrode's performance surpassed that of conventional Pd/C powder electrodes, suggesting that electrode morphology and the electrochemical environment play a crucial role in determining fuel cell efficiency. Lastly, the integration of reduced graphene oxide (rGO) with CoNi nanosheets array on Ni foam (CoNi/rGO@Ni foam) has been shown to offer impressive catalytic performance for urea electrooxidation.[131] This synergy between graphene and metal nanosheets could potentially redefine electrode designs, paving the way for next-generation FCs.

Recent advancements in FC research have unveiled the potential of Pt/Ir(111) bimetallic surfaces, which demonstrate a balance between enhanced hydrogen oxidation reaction (HOR) activity and suppressed hydrogen peroxide generation. This study elucidates the relationship between Pt and Ir surface sites. It suggests that these bimetallic surfaces could serve as anode catalysts for polymer electrolyte FCs, potentially enhancing their performance.[132] Building on this, the introduction of 3D Ni and Co@TiC nanoarrays as anodes in direct peroxide-peroxide FCs leads to increased performance. Nanoarrays empirical performance metrics, particularly peak power densities and cell stability, underscore their potential to redefine FCs' applications.[102]

Furthermore, studies on Ni-Pd core-shell nanoparticles and microfiber cathodes in magnesium-$H_2O_2$ semi-FCs have provided insights into their respective applications, with a focus on their unique fabrication techniques and performance metrics. In another study, the impact of Ni-Metal core-shell nanoparticles on multiwalled carbon nanotube (MWCNT) support was explored, specifically for borohydride oxidation in alkaline solutions. Among the tested combinations, Ni@Pd/MWCNT emerged as the most efficient, showcasing the highest borohydride oxidation current density. This combination surpassed other materials in terms of energy conversion efficiency and power density in direct borohydride-$H_2O_2$ FCs.[133] Strontium doping of lanthanum manganese oxide (La1-xSrxMnO$_3$ $\pm\sim\delta$) was investigated as a potential catalyst for hydrogen peroxide reduction reaction (HPRR)

in alkaline solutions. While the Sr-doped variant outperformed its undoped counterpart, it still lagged behind platinum-based catalysts in terms of activity.[134] A standout research is the development of the Ag-$W_2C$/C electrocatalyst, which was prepared using an intermittent microwave heating method. This catalyst has demonstrated high selectivity for oxygen reduction, especially in the presence of alcohol. Such selectivity suggests promising applications for mixed-reactant anion exchange membrane FCs. The overarching implication of this study is the potential enhancement in energy density and cost reductions that can be achieved by employing highly selective catalysts.[135] In the pursuit of innovative catalyst designs, a study introduced a pineapple root-like palladium-gold catalyst tailored for direct peroxide-peroxide FCs. This catalyst was synthesized by electro-depositing palladium and gold onto a titanium carbide nanowire array substrate. The resultant $Pd_5Au_1$/TiC electrode showcased remarkable electrochemical properties and stability. Notably, the fuel cell equipped with this electrode achieved an open circuit voltage of 0.85 V and a peak power density of 56.5 mW $cm^{-2}$, figures that surpass previously reported values.[136] Shifting focus to the performance of $H_2O_2$ FCs (HPFCs), a study highlighted the potential of PEDOT as a cathodic catalyst. The research underscored that PEDOT does not induce peroxide disproportionation and competes favorably with some of the leading inorganic catalysts. This suggests avenues for enhancing the performance and stability of HPFCs, either by optimizing PEDOT formulations or by exploring other conducting polymers.[25] The intricate interplay of catalyst selection, structural design, and operational parameters is pivotal in determining fuel cell efficiency. The findings from these studies not only underscore the rapid advancements in the field but also emphasize the significance of material science, electrochemistry, and engineering design in propelling sustainable energy solutions.

A notable advancement is the development of a prototype $H_2O_2$-fuel cell that employs a mesoporous anatase $TiO_2$ nanocrystalline film as the photoanode. Under UV-light irradiation, this cell showcased a short-circuit current of 0.24 mA $cm^{-2}$ and an open-circuit voltage of 0.72 V. Interestingly, a response to visible light was also observed, attributed to the charge-transfer complex formation of $H_2O_2$ on the $TiO_2$ surface. The FC's estimated maximum power-generating efficiency reached an impressive 79%.[137] A study introduced a petal-shaped Co/$Co_3O_4$ composite electrocatalyst, synthesized through hydrothermal methods and in situ chemical reduction. This catalyst displayed superior conductivity and catalytic activity for $H_2O_2$ electroreduction compared to singular $Co_3O_4$, marking it as a promising alternative catalyst for $H_2O_2$ FCs.[138] Subsequent studies used the potential of various catalysts and materials, such as platinum on hydrogen peroxide-treated carbon black, nanoporous carbon-supported palladium-zinc nanocomposites, and a carbon-supported bimetallic Au-Pd catalyst. Subsequent studies provided insights into the performance, stability, and catalytic activity of these materials in fuel cell applications.[139,140]

Bimetallic nanoparticles, especially when supported on nitrogen-doped reduced graphene oxide (N-rGO), have emerged as a promising avenue in electrocatalysis for fuel cell applications. A notable study showcased the synthesis of Pd-X (where X = Ni, Co) nanoparticles on N-rGO using a unique combination of a solid-state thermal technique followed by polyol reduction. The results from this research were particularly enlightening. The Pd-Ni/N-rGO catalyst displayed superior electrochemical performance in borohydride oxidation in alkaline solutions when compared to its counterpart, Pd-Co/N-rGO. This superiority manifested in the form of a higher current density, enhanced stability, and a more negative onset potential. Furthermore, in the context of a direct sodium borohydride-hydrogen peroxide fuel cell, the Pd-Ni/N-rGO catalyst outshone by achieving a peak power density of 353.84 mW $cm^{-2}$ at 60 °C, clearly outperforming the Pd-Co/N-rGO variant.[141]

The integration of photochemistry in FC technology is evident in the photo-assisted FC design using dual photoelectrodes under tandem illumination, which ensures enhanced charge separation and light absorption.[142] The DPPFC's novel approach of using $H_2O_2$ as both fuel and oxidant simplified the fuel cell design, emphasizing the cost-effectiveness of $H_2O_2$ and the importance of non-precious metals in catalysts.[143] The composite of nickel/nickel oxide on nitrogen-doped graphene highlighted the potential of hybrid materials in electrocatalysis.[97] The self-supported DBHFC system's peak power output under ambient conditions showcased its potential for specialized applications.[144]

## 8. Membraneless Laminar Flow-Based (Microfluidic) Fuel Cell

The utilization of microfluidics is pivotal in advancing $H_2O_2$ FC technology, effectively addressing contemporary trends and challenges within the field. Microfluidic devices enable precise manipulation and control of fluid flow, ensuring uniform dispersion of reactants and products within the fuel cell. This precision enhances reaction kinetics, optimizing overall performance and meeting the increasing demand for efficient and sustainable energy solutions. LFFC approaches, when applied to membraneless $H_2O_2$ FCs, offer distinct advantages beyond the mere absence of a membrane. The LFFC design capitalizes on the laminar flow regime to segregate reactant streams, thereby minimizing crossover and enhancing fuel utilization. This controlled flow within microchannels ensures precise reactant delivery, potentially optimizing reaction kinetics. Furthermore, the microscale architecture of LFFCs allows for a compact and efficient design, which can be critical for applications demanding portability and rapid response. While $H_2O_2$ FCs inherently operate without membranes, the incorporation of LFFC principles can further refine their operational efficiency and adaptability. Microfluidics plays a pivotal role in the development and optimization of FCs, especially those utilizing $H_2O_2$ as both fuel and oxidant. The integration of microfluidic principles in a membraneless fuel cell with a Y-shape channel led to a comprehensive model that simulated fluid flows, mass transport, electrochemical kinetics, and charge transport. This model, deeply rooted in microfluidic dynamics, highlighted the effects of oxygen gas produced on the anode electrode on cell performance and the mixing zone, offering a clear understanding of the interplay between microfluidic behavior and electrochemical processes.[145]

The importance of microfluidics is further emphasized in the exploration of innovative electrode designs since, microfluidic platforms facilitate miniaturization and integration of $H_2O_2$ FC systems, rendering them suitable for portable

and decentralized power generation applications. Additionally, the use of microfluidic-based manufacturing processes offers cost-effective and scalable production methods for $H_2O_2$ FC components, addressing challenges related to scalability and affordability. Moreover, the incorporation of microfluidic sensors and diagnostics allows for real-time monitoring of $H_2O_2$ FC performance, enabling proactive maintenance and optimization strategies to improve system reliability and longevity.

In the field of this approach, a fuel cell that employed Prussian blue coating on carbon paper as the cathode and a three-dimensional flow-through Ni foam as the anode was developed. The microfluidic design principles were crucial in achieving notable power density, although the corrosion of Ni foam in $H_2O_2$ remained a concern.[146] Another design, which integrated nickel nanoparticles and Prussian blue with multiwalled carbon nanotube coated on hydrophilic braided carbon fibers as electrodes, leveraged microfluidic dynamics to deliver high power density and superior stability.[147] Microfluidics also played a central role in the development of FCs constructed with novel materials. A laser-micromachined polymeric membraneless fuel cell, constructed with three polymethyl methacrylate layers, showcased stable operation across varying Reynolds numbers, underscoring the significance of microfluidic principles in its design.[148] Paper-based FCs, inherently reliant on microfluidic dynamics, have been explored extensively. One such design powered by urea was constructed on filter paper, emphasizing the importance of microfluidic behavior in paper substrates.[149] Another paper-based design utilized silver nanowires and carbon nanotube-supported Prussian Blue as catalysts, with microfluidics playing a crucial role in its operation.[150] Reviews on membraneless microfluidic fuel cells (MMFCs) have emphasized the role of microfluidics in categorizing these cells based on design, components, and utility, offering insights into the challenges and future prospects for MMFC commercialization.[151]

Microfluidic FCs, particularly those utilizing $H_2O_2$ as both fuel and oxidant, have garnered significant attention due to their potential in portable and wearable devices. These FCs offer a unique combination of compactness, efficiency, and flexibility, making them ideal for a range of applications. Also for such type FCs, a study of a 3D, two-phase model for a membraneless fuel cell with a Y-shaped microchannel was provided. Besides, the simulation model for the operation of the fuel cell using $H_2O_2$ dissolved in diluted NaOH and $H_2SO_4$ solutions was presented. The model's validation with experimental data showed good agreement, and it was found that the presence of the gas phase (oxygen) acts to prevent the processes of reactant supply and product removal. The study also revealed that the current density distribution is influenced by mass transfer and electrochemical kinetics. The maximum power density achieved by this fuel cell was 0.22 mW $cm^{-2}$ at a current density of 0.18 mA $cm^{-2}$.[152] Another experimental study reported the performance of a low-cost paper-based membraneless DHPFC. The optimal conditions for this cell were found to be 5 mol $L^{-1}$ KOH, 2 mol $L^{-1}$ $H_2O_2$, and 40 °C, which yielded an open circuit voltage of 0.87 V and a peak power density of 6.79 mW $cm^{-2}$.[153] Similarly, an analysis of a membraneless microfuel cell in a Y-shaped microchannel was presented. This cell also used nickel foam coated with specific catalysts as electrodes. Under optimal conditions, the cell achieved an open circuit voltage of 0.87 V and a peak power density of 6.79 mW $cm^{-2}$.[154] A unique paper-based membraneless hydrogen peroxide fuel cell was introduced, which was fabricated using photosensitive glass wafers and thermal bonding. This fuel cell maintained a stable OCP of 0.61 V and a maximum power density of 0.81 mW $cm^{-2}$ at 0.26 V, even after distortion. The fuel cell demonstrated its capability to power devices like LEDs and LCDs using $H_2O_2$ as the sole power source.[155] A comprehensive review of paper-based microfluidic FCs (PMFCs) highlighted their potential as a power source for portable devices. These PMFCs rely on the capillary-driven co-laminar flow of fuel and oxidant streams in a porous paper substrate. The review also discussed the various fuels and oxidants used in PMFCs, their advantages and disadvantages, and stacking techniques to increase voltage and power output.[11]

The presence of $O_2$ bubbles in $H_2O_2$ FCs is a critical factor influencing the laminar flow regime, thereby impacting fuel cell performance. In laminar flow conditions, $O_2$ bubbles disrupt fluid flow patterns, leading to non-uniform reactant distribution and concentration gradients, which can affect reaction rates and overall FC performance. Additionally, interactions between $O_2$ bubbles and the liquid electrolyte influence gas-liquid interface dynamics and mass transport processes, further complicating fuel cell operation. A study estimated the gas production rate from such cells and found that $O_2$ bubbles are likely to be generated under specific conditions. The bubble growth rate in a given microfluidic fuel cell was found to be almost constant at different regions of that cell at a given volumetric flow rate.[156] A novel approach introduced a valveless impedance pump for supplying liquid fuels to a direct sodium borohydride—hydrogen peroxide fuel cell (DBHPFC). When connected to a DBHPFC, the pump could deliver fuel at a maximum rate of 30 $mlmin^{-1}$, resulting in a DBHPFC maximum power of 13.0 W and current of 25.5 A.[157] Another experimental study of direct hydrogen peroxide microfluidic FCs investigated the effects of various factors on performance. The highest cell current density output at 0.1 V and 0.6 M was 250 mA $cm^{-2}$.[158] A research paper described a flexible microfluidic fuel cell using $H_2O_2$ as the sole reactant. This cell achieved a power density of 2.22 W $m^{-2}$ with a current density of 7.64 $Am^{-2}$.[159] Another study focused on the effect of bubbles in microfluidic FCs, revealing that bubbles could be a dominant factor in cell performance. The study suggested that future research could focus on novel microfluidic fuel cell designs to reduce bubble formation.[160] The transition between laminar and turbulent flow regimes, triggered by bubble formation, introduces additional complexities, including energy losses and pressure drops, which can influence FC efficiency. Moreover, excessive bubble accumulation near the electrode surface can lead to electrode flooding, hindering mass transport and reducing active surface area for electrochemical reactions. A single-stream $H_2O_2$ membraneless microfluidic fuel cell that uses cotton threads for reactant solution transport is shown. This fuel cell produced a maximum power density of 5.5 mW $cm^{-2}$ with an open-circuit potential value of 0.66 V.[161] LFFCs, especially those utilizing $H_2O_2$, present a promising avenue for efficient, compact, and flexible energy solutions. Therefore, mitigation strategies, such as optimizing flow channel designs and controlling operating conditions, are essential to address existing challenges and optimize $H_2O_2$ FC performance.

Another study describes a high-performance hydrogen peroxide fuel cell (HPFC) that uses buckypaper and a narrow fuel pathway. The authors found that the HPFC generated 2.32 kW $m^{-3}$ in municipal stationary operation with solar-driven $H_2O_2$ fuel or cascade reaction-based implantable biodevices. Authors' work also discusses the effects of cobalt phthalocyanine and polyacrylic acid on the reactivity of hydrogen peroxide oxidation reaction and the performance of hydrogen peroxide fuel cell. Results demonstrate the potential of HPFCs as a sustainable energy source. Similar to one-compartment FCs, membraneless LFFCs operate without the use of a proton-conducting membrane. The main advantage of LFFCs is the spatiotemporal separation of fuel and oxidant using laminar co-flows. The ultimate aim is to increase the performance of $H_2O_2$ LFFCs by enhancement of mass transport rates using integrated autonomous micropumps. In portable devices, energy density often takes precedence over efficiency because of the modest power demands. Under laminar flow, two fluids mainly interact through diffusion, limiting their mixing.[145] $H_2O_2$ stands out in FC applications because it can undergo both oxidation and reduction, each at distinct electrochemical potentials (NHE). This suggests the potential to employ $H_2O_2$ as both the fuel and oxidizer in the same FC. The proposition of the membrane-less FCs and flow-through porous electrodes architecture[162] lead to a number of studies following the trend of such simple and efficient LFFCs design. Moreover, as pointed by Zhu et al. such fuels as vanadium redox species used in many studies may reduce the cell flexibility due to the environmental concerns.[163]

The overall performance of the cells depends on many parameters, such as design and geometry, fuel, electrode type and materials used as catalysts, etc. There are several reviews and perspectives devoted to various aspects of a great family of microfluidic FCs.[151,164–170] As fuel and oxidant, catalyst also play an important role. FCs electrodes and materials are well-discussed in review of Rashed et al.[171] Some attention to the electrode materials is made by Hanapi et al.[172] According to Yang et al. noble-metal catalysts like Pt, Au, and Pd–Ir alloy are always selected to catalyze the $H_2O_2$ decomposition.[146] Pt is often used as a catalyst in air-breathing cathode.[173] In many cases, Pt is used for cathode, while Pd can be a anode, see **Table 1**. Typically, the fabrication of the anode and cathode involves a carbon based materials as substrate due to high electrical conductivity, chemical stability, and thermal stability.[174] Nonetheless, carbon materials primarily serve as a support for catalysts. Most popular support is carbon paper, utilized by Wu et al.[175] and Zhou et al.[176] Besides, many studies employ graphite, carbon fibers and carbon nanotubes as a catalyst support. Although, carbon materials, e.g., carbon nanotubes or other, are very conductive and usually are characterized by great specific surface, they are also rather hydrophobic. Appearing gas bubbles might not detach from their surface easily that leads to blocking the surface and decrease of fuel cell performance. To address this problem, such materials are modified by various treatment ways to make it more hydrophilic, e.g., as in the following papers.[173,174] R.S. Jayashree et al.[69] designed air-breathing laminar flow-based microfluidic fuel cell with Pt electrodes, i.e., Pt nanoparticles on graphite and carbon paper. Some studies demonstrate that Ni mesh, Ag nanowires might be applied as anodes without use of Pd, Pt of Ru materials. Some cathodes might employ Prussian blue and multiwalled carbon nanotubes-coated carbon cloth[161] or $CN_x$ nanofibers[177] that makes them noble metal free. Yet, noble metal free cells are just about to be further designed that requires search for new catalysts and fuel/oxidant systems. Interestingly, pure carbon electrodes are employed in FCs that include membrane. As discussed by the O. Muneeb et al., alkaline direct liquid FCs helped to reduce dependence on Pt, while the use of Pd still remained.[178] But, the authors, took advantage of making an ascorbate fuel cell with carbon black nanoparticles as both anode and cathode, though, with anion exchange membrane (or $Na^+$ treated cation exchange membrane). Ascorbate and KOH are used as fuel, cathode oxidant was $O_2$ or $H_2O_2$ to give the maximum power density 16 mW $cm^{-2}$ (OCV 0.53 V, 0.39 V). Using the cation exchange membrane with ascorbate and KOH as anode fuel stream and $H_2O_2$ and $H_2SO_2$ as cathode oxidant stream a power density of 158 mW $cm^{-2}$ (OCV 1.29-1.31 V) is reached. A study by Campos-Roldán[179] utilized gaseous oxygen and hydrogen as oxidant and fuel, respectively, i.e., gaseous fuel in microfluidic cell. The authors managed use platinum metal free electrodes and achieved the 15 mW $cm^{-2}$ maximum peak power. In the cell design, a microchannel with KOH solution was realized, while gases were supplied as flow over "breathing"-like electrodes.

## 9. Integration of Valveless Catalytic Micropumps

Integrating valveless catalytic micropumps into membraneless $H_2O_2$ FCs offers the distinct advantage of reducing energy consumption. These micropumps eliminate the need for external pumps, which are typically energy-intensive. By simplifying the system, not only is energy efficiency enhanced, but the overall design becomes more compact and less complex. The valveless design of pumps minimizes mechanical complexity, potentially reducing maintenance needs and increasing the durability and reliability of the FCs. The reduction in energy requirements not only improves the operational efficiency of the FCs, but also can contribute to their sustainability, making FCs more suitable for applications where energy availability is a critical concern. **Figure 5a** shows main principles of $H_2O_2$ catalytic micromotor self-propelled by self-electrophoresis in $H_2O_2$ solution. Autonomous pump operating in the same chemical fuel by electrokinetic phenomena is shown in Figure 5b. Figure 5c depicts a typical $H_2O_2$ LFFCs with co-laminar flows.[30] Figure 5d illustrate an electrokinetic pumping mechanism integrated in thin film $H_2O_2$ FC's architecture,[21] using advantages of fluid/fuel autonomous transport shown for dead-end pores.[184]

Bubbles in $H_2O_2$ FCs block active surface area of electrodes, leading to a lower FCs' performances. The addition of surfactants to the solution changes the interfacial properties of the fuel/oxidant, which can enhance the wettability of the electrodes, increase the electrode's effective surface area, eject microbubbles and thereby increase the rate of the reactions. To achieve pumping, a highly efficient $O_2$ bubble-driven micropump decomposing $H_2O_2$ as low as $10^{-4}$% was developed.[20] The micropump has an efficiency of $O_2$ microbubbles nucleation in several orders magnitude higher than planar catalytic surfaces and larger catalytic pumps. Bubble-driven micropump based on rolled-up catalytic microtube is shown in **Figure 6a**.

**Table 1.** Fuel, oxidant, cathode, anode, reactions, OCP and peak power density of different hydrogen peroxide powered FCs.

| Type of fuel cell | Fuel | Oxidant | Cathode | Reaction (cathode) | Anode | Reaction (anode) | OCP | Peak power density | Ref. |
|---|---|---|---|---|---|---|---|---|---|
| Microfluidic | $H_2O_2$ | $H_2O_2$ | carbon nanotube-supported Prussian Blue | $H_2O_2 + 2H^+ + 2e \rightarrow 2H_2O$ ($E^0 = 1.77$ V vs. SHE) | silver nanowires | $H_2O_2 \rightarrow 2H^+ + 2e + O_2$ ($E^0 = 0.682$ V vs. SHE) | 1.09 V (theoretical), 0.58 V (practical) | 0.88 mW cm$^{-2}$ | [150] |
| Microfluidic fuel cell | $H_2O_2$ | $H_2O_2$ | carbon paper supported Prussian Blue, Nafion | $H_2O_2 + 2H^+ + 2e \rightarrow 2H_2O$ ($E^0 = 1.77$ V vs. SHE) | Ni foam | $H_2O_2 \rightarrow 2H^+ + 2e + O_2$ ($E^0 = 0.68$ V vs. SHE) | 0.65 V | $0.58 \pm 0.13$ W m$^{-2}$ | [146] |
| Membrane- less microfluidic fuel cell | $H_2O_2$ | $H_2O_2$ | Prussian blue (PB) and multiwalled carbon nanotubes-coated carbon cloth | $H_2O_2 + 2H^+ + 2e \rightarrow 2H_2O$ ($E^0 = 1.77$ V vs. SHE) | Ni mesh | $H_2O_2 \rightarrow 2H^+ + 2e + O_2$ ($E^0 = 0.68$ V vs. SHE) | 0.66 V | 5.5 mW cm$^{-2}$ | [161] |
| Direct hydrogen peroxide fuel cell | $H_2O_2$ in NaOH | $H_2O_2$ in $H_2SO_4$ | Pt | $H_2O_2 + 2H^+ + 2e \rightarrow 2H_2O$ ($E^0 = 1.763$ V) | Pt | $H_2O_2 + OH^- \rightarrow HO_2^- + H_2O$, $HO_2^- + OH^- \rightarrow O_2 + H_2O + 2e$ ($E^0 = 0.0649$ V) | 0.7 V | 23 mW cm$^{-2}$ | [180] |
| Microfluidic direct formate fuel cell | HCOOK with or without KOH | 30% $H_2O_2$ or 3% $H_2O_2$ with 0.5 M KCl | small dots (3 mm diameter) of colloidal graphite | $HO_2^- + 2e + H_2O \rightarrow 3OH^-$, $E_{0(cathode)} = 0.88$ V | small dots (3 mm diameter) of 30wt% Pd/C | $HCOO^- + 3OH^- \Leftrightarrow CO_3^{2-} + 2H_2O + 2e^-$, $E_{0(anode)} = -1.05$ V | > 1 V | 2.5 mW mg$^{-1}$Pd | [181] |
| Alkaline direct formate paper microfluidic fuel cell | 5 M HCOOK | 30% $H_2O_2$ | activated carbon catalyst with Nafion | [Reduc- tion of $H_2O_2$] | Pd on carbon | [Oxidation of formate] | 0.9, 1.8, and 2.4 V for a single, double, and triple cell configuration, respectively | 2.53 mW cm$^{-2}$ | [182] |
| Microfluidic FCs | sodium formate and potassium hydroxide as the electrolyte and supporting electrolyte | $O_2$ and potassium hydroxide as the electrolyte and supporting electrolyte | Pt black and Nafion on carbon paper (Toray 090) | [Reduc- tion of oxygen to hydroxide ions] | Pd electrodeposited on carbon paper (Toray 090), Nafion | [Oxidation of formic acid to carbon dioxide, releasing electrons] | 1.04 V | 119.3 mW cm$^{-3}$ | [176] |
| Laminar flow, microfluidic | 0.2 M HCOOH in 0.5 M sulfuric acid | 0.01 M $H_2O_2$ in 0.5 M sulfuric acid | Pt | $H_2O_2 + 2H^+ + 2e \rightarrow 2H_2O$ | Pt | $HCOOH^+_{(aq)} \rightarrow CO_{2\,(g)} + 2H^+_{(aq)} + 2e^-$ | 0.32 V | 94.8 μ cm$^{-2}$ | [183] |

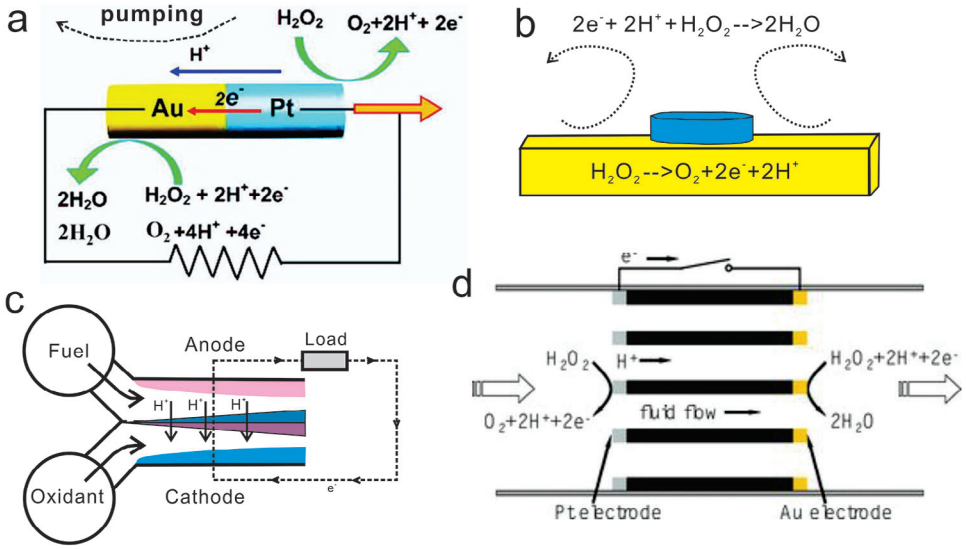


**Figure 5.** a) Catalytic nanomotor consisted of a bimetallic Au-Pt nanorod. Oxidation-reduction reactions result in the transport of electrons in metals and protons at the solid–$H_2O_2$ fuel interface. Simultaneously, in catalytic micropump mobile protons drag water molecules and lead to the self-pumping principle. Reproduced with permission.[185] Copyright 2020, IntechOpen. b) Schematic image of catalytic micropump operating by the same chemical priciple as catalytic nanomotors. c) Schematic image of a typical LFFC, where fuel and oxidant are spatiotemporally separated at a low Reynolds number. Adapted with permission.[30] Copyright 2004, Elsevier. d) A novel appraoch to integrate electrokinetic micropump in thin film porous membrane FC. Reproduced with permission.[21] Copyright 2010, John Wiley and Sons.

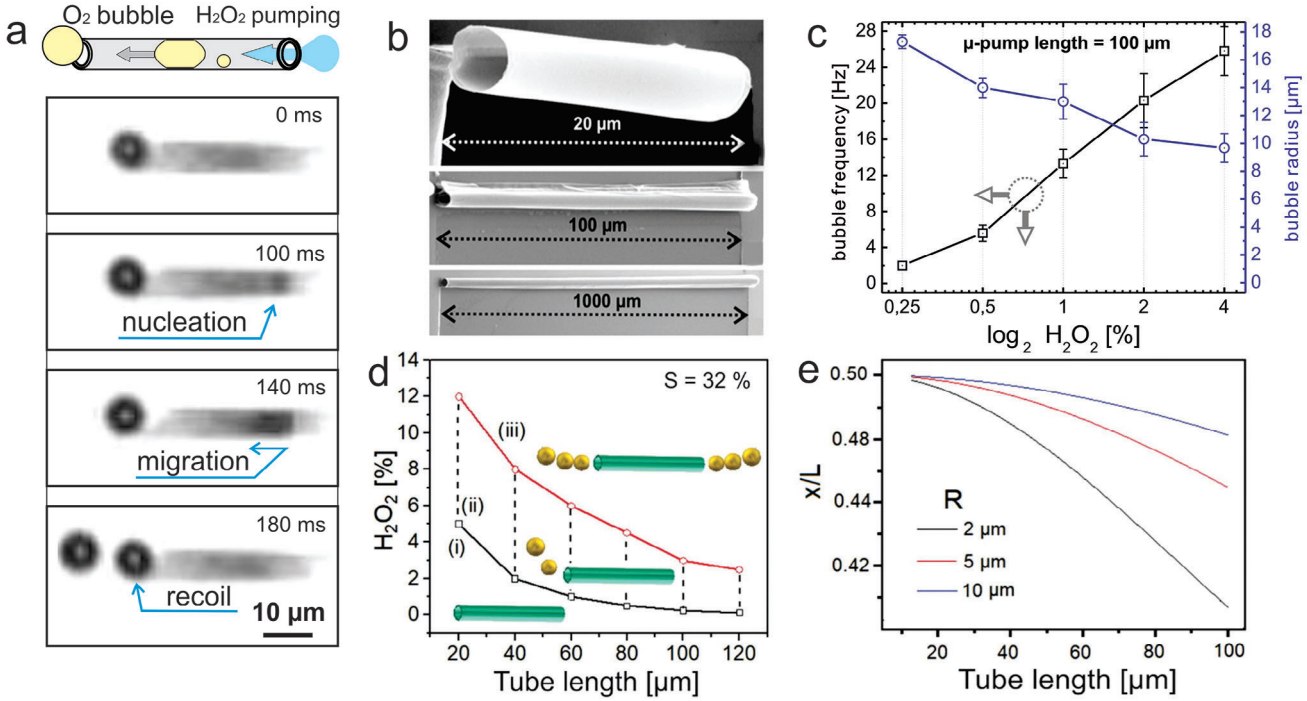


**Figure 6.** a) Schematic image and optical micrograph image sequences of tubular bubble-driven micropump powered by decomposition of $H_2O_2$. Reproduced with permission.[186] Copyright 2012, MONARCH Online Database. b) Optical micrograph of a catalytic tubular micropump with different lengths ranging from 20 to 1000 μm, operated by the $O_2$ bubble recoil. Reproduced with permission.[186] Copyright 2012, MONARCH Online Database. c) Dependence of oxygen bubbles frequency and diameter on $H_2O_2$ concentration (for 10 μm diameter, 100 μm length pumps). Reproduced with permission.[20] Copyright 2011, Royal Society of Chemistry. d) Study of microbubbles generation (unidirectional, bidirectional ejection) for tubes with different lengths immersed in various concentrations of $H_2O_2$. Adapted with permission.[187] Copyright 2019, AIP Publishing. e) Theoretical simulation: bubble nucleation point dependence on the aspect ratio of the tubular micropump; for the maximum concentration of oxygen, versus *L* for different radii. Adapted with permission.[187] Copyright 2019, AIP Publishing.

Physicochemical properties, including $H_2O_2$ fuel concentration, surfactants concentration (surface tension), catalytic microchannel aspect ratio, were optimized and full control over the $O_2$ bubble nucleation/generation was achieved (Figure 6b–d). Subsequently, oxygen nucleation and generation in tubular micropumps have been supported by theoretical modeling of reaction-diffusion processes. It is shown how bubble nucleation point shifts along the tube's axis of symmetry depending on tube's aspect ratio, indicated in Figure 6e.[20]

The developed theoretical model predicts an amount of generated oxygen gas, bubble recoil at one tubular opening (i.e., "unidirectional regime") and two tubular openings (i.e., "overloaded regime").[187] A 1D reaction-diffusion equation was formulated to describe the mass transport in catalytic tubes. A position of the maximum oxygen concentration can be found by the following equation:

$$x_{max} = \frac{1}{\beta} sinh^{-1}\left(\frac{1}{\beta L}\left(1 - cosh(\beta L)\right) + \frac{L}{2}\right) \quad (14)$$

where $\beta = (\frac{2k}{D_{H_2O_2} R})^2$, $k$ is the reaction constant ($k = 6.83 \times 10^{-7} ms^{-1}$), $D_{H_2O_2} = 1.43 \times 10^{-9} m^2 s^{-1}$ is the diffusion constant of hydrogen peroxide, $R$ is the radius of the tube, and $L$ is the length of the tube. Using tubular length and radius, the concentration of hydrogen peroxide fuel and calculated beta coefficient theoretical value of the total produced oxygen mass can be calculated with a close consistency with experimental values $10^{-13}$–$10^{-14}$ kg $s^{-1}$. In the context of $H_2O_2$ FCs and LFFCs, the model's significance extends especially to the development of thin film and porous electrode-based cells, where precise mass transport is crucial. The model's accuracy in predicting oxygen generation and bubbles' behaviors is key parameter for advanced designs, enhancing FCs' overall efficiency and effectiveness.

## 10. Conclusion and Outlook

The successful development of $H_2O_2$ FCs holds significant promise in contributing to global carbon emission reduction and the transition to a carbon-neutral economy. Addressing the challenges in optimizing electrocatalysts, fuel/oxidant compositions, and architectures for these FCs is critical. The elimination of a physical electrolytic membrane opens the pathway for developing single compartment FCs, which are both economically and spatially efficient. A primary concern is the tendency of metallic electrodes to catalyze the disproportionation of $H_2O_2$ into $O_2$ and $H_2O$, impacting the electrochemical efficiency. The deviation of the observed reduction reaction of $H_2O_2$ from its theoretical OCP, due to concurrent oxidation reactions at the cathode, requires further investigation. Elevated concentrations of hydrogen ions and hydroperoxyl radicals may accelerate $H_2O_2$ decomposition, necessitating additional empirical studies to understand these effects fully. The integration of microfluidic LFFCs with $H_2O_2$ FCs can potentially offer intriguing possibilities. LFFCs, with their inherent laminar flow dynamics, provide a sophisticated mechanism for enhancing reactant segregation, reducing crossover phenomena and optimizing the electrochemical interface in $H_2O_2$ FCs. However, challenges such as scalability and managing operational pressures in microscale architectures must be addressed. Valveless autonomous micropumps and self-powered electrokinetic/osmotic pumps present potential solutions for these challenges. LFFCs, operating at the microscale, face inherent limitations in larger-scale applications due to pronounced crossover phenomena. Thin-film FC can boast several significant advantages, primarily due to their high surface area-to-volume ratio, which enhances the efficiency of electrochemical reactions and mass transport. This increased surface area allows for more effective catalyst utilization, leading to improved reaction kinetics and higher power densities compared to bulkier counterparts. Exploring redox couples and combining peroxide with other fuels such as ethanol, formic acid, and metals like magnesium could expand the utility of these FCs in a unified architecture. The integration of $H_2O_2$-powered valveless micropumps and membraneless FCs is increasingly recognized for its potential to bring about significant economic benefits. These benefits include reductions in manufacturing costs due to simpler device architectures, improvements in energy efficiency achieved through direct fuel utilization, and enhancements in system performance attributable to the elimination of complex supporting infrastructure. Additionally, the deployment of $H_2O_2$ FCs opens up new market opportunities by catering to niche applications, where traditional FCs are impractical, such as in portable medical devices, underwater vehicles, and aerospace applications, further driving the appeal of this technology. Sustainability benefits are also a key consideration, with $H_2O_2$ FCs offering a cleaner alternative to fossil fuel-based energy sources, contributing to reduced greenhouse gas emissions and promoting environmental stewardship. The path to realizing the full potential of $H_2O_2$ FC technology hinges on dedicated, interdisciplinary research efforts. Advancements in materials science are particularly critical, with research focusing on the development of more durable, selective electrocatalysts that can withstand the harsh operational conditions of $H_2O_2$ decomposition while maintaining high activity levels. Refining device design to incorporate features such as integrated bubble management and improved electrode architectures can further elevate the performance and reliability of $H_2O_2$ FCs. The development of computational models and simulation tools to predict fuel cell behavior under various operational conditions can accelerate the design optimization process, reducing the time and cost associated with experimental testing. Collectively, these research and development efforts are crucial for overcoming the existing barriers to $H_2O_2$ FC adoption, ensuring that this innovative technology can achieve widespread, practical utility and establish a competitive position in the global energy market. As the field continues to evolve, the collaborative endeavors of scientists, engineers, and industry stakeholders will be instrumental in harnessing the unique advantages of $H_2O_2$ FCs, driving forward the transition to a more sustainable and efficient energy landscape. In conclusion, the ongoing research and development in $H_2O_2$ FC technology, particularly in membraneless designs, is forging a path toward their practical application as dynamic electrochemical agents. Persistent and collaborative research efforts, focusing on advancing materials, improving mass transport, and refining device design, are crucial for achieving widespread, practical utility of $H_2O_2$ FC's technology.

## Acknowledgements

This work was supported by the National Key Technologies R&D Program of China (2021YFA0715302 and 2021YFE0191800), the National Natural Science Foundation of China (61975035 and 52150610489), the Science and Technology Commission of Shanghai Municipality (22ZR1405000) and the Ministry of Science and Higher Education of the Russian Federation (FSME-2022-0008).

## Conflict of Interest

The authors declare no conflict of interest.

## Keywords

electrocatalysts, fuel cells, hydrogen peroxide, laminar flow, membraneless

Received: November 30, 2023
Revised: April 16, 2024
Published online: June 12, 2024

[1] S. A. M. Shaegh, S. M. M. Ehteshami, S. H. Chan, N.-T. Nguyen, S. N. Tan, *RSC Adv.* **2014**, *4*, 37284.
[2] K. Mase, M. Yoneda, Y. Yamada, S. Fukuzumi, *Nat. Commun.* **2016**, *7*, 11470.
[3] L. An, T. Zhao, X. Yan, X. Zhou, P. Tan, *Sci. Bull.* **2015**, *60*, 55.
[4] C. J. McDonnell-Worth, D. R. MacFarlane, *Aust. J. Chem.* **2018**, *71*, 781.
[5] Y. Yamada, M. Yoneda, S. Fukuzumi, *Inorg. Chem.* **2014**, *53*, 1272.
[6] S. Fukuzumi, Y. Yamada, *ChemElectroChem* **2016**, *3*, 1978.
[7] G. H. Miley, N. Luo, J. Mather, R. Burton, G. Hawkins, L. Gu, E. Byrd, R. Gimlin, P. J. Shrestha, G. Benavides, J. Laystrom, D. Carroll, *J. Power Sources* **2007**, *165*, 509.
[8] S. A. M. Shaegh, N.-T. Nguyen, S. M. M. Ehteshami, S. H. Chan, *Energy Environ. Sci.* **2012**, *5*, 8225.
[9] S.-i. Yamazaki, Z. Siroma, H. Senoh, T. Ioroi, N. Fujiwara, K. Yasuda, *J. Power Sources* **2008**, *178*, 20.
[10] E. Kjeang, A. G. Brolo, D. A. Harrington, N. Djilali, D. Sinton, *J. Electrochem. Soc.* **2007**, *154*, B1220.
[11] M. Tanveer, T. Ambreen, H. Khan, G. M. Kim, C. W. Park, *Energy Convers. Manage.* **2022**, *264*, 115732.
[12] L. An, T. Zhao, X. Zhou, L. Wei, X. Yan, *RSC Adv.* **2014**, *4*, 65031.
[13] L. An, T. Zhao, X. Zhou, X. Yan, C. Jung, *J. Power Sources* **2015**, *275*, 831.
[14] Y. Yang, R. Dong, Y. Zhu, H. Li, H. Zhang, X. Fan, H. Chang, *Chem. Eng. J.* **2020**, *381*, 122749.
[15] Y. Yang, H. Zhang, J. Wang, S. Yang, T. Liu, K. Tao, H. Chang, *J. Mater. Chem. A* **2019**, *7*, 11497.
[16] P. Forysinski, C. Oloman, S. Kazemi, T. Nickchi, A. Usgaocar, *J. Power Sources* **2019**, *414*, 366.
[17] A. A. Solovev, Y. Mei, E. Bermúdez Ureña, G. Huang, O. G. Schmidt, *Small* **2009**, *5*, 1688.
[18] T. R. Kline, W. F. Paxton, Y. Wang, D. Velegol, T. E. Mallouk, A. Sen, *J. Am. Chem. Soc.* **2005**, *127*, 17150.
[19] S. Naeem, F. Naeem, J. Liu, V. A. B. Quiñones, J. Zhang, L. He, G. Huang, A. A. Solovev, Y. Mei, *Chem.–An Asian J.* **2019**, *14*, 2431.
[20] A. A. Solovev, S. Sanchez, Y. Mei, O. G. Schmidt, *Phys. Chem. Chem. Phys.* **2011**, *13*, 10131.
[21] I.-K. Jun, H. Hess, *Adv. Mater.* **2010**, *22*, 4823.
[22] S. Naeem, F. Naeem, J. Mujtaba, A. K. Shukla, S. Mitra, G. Huang, L. Gulina, P. Rudakovskaya, J. Cui, V. Tolstoy, et al., *Micromachines* **2021**, *12*, 1251.
[23] S. Jeon, H. An, Y. Chung, *Sustainable Energy Fuels* **2022**, *6*, 841.
[24] S. Fukuzumi, Y. Yamada, K. D. Karlin, *Electrochim. Acta* **2012**, *82*, 493.
[25] E. Miglbauer, P. J. Wójcik, E. D. Głowacki, *Chem. Commun.* **2018**, *54*, 11873.
[26] G. Shi, D. A. Tryk, T. Iwataki, H. Yano, M. Uchida, A. Iiyama, H. Uchida, *J. Mater. Chem. A* **2020**, *8*, 1091.
[27] N. Dhanda, Y. K. Panday, S. Kumar, *Electrochim. Acta* **2024**, *481*, 143872.
[28] Y. H. Hong, Y.-M. Lee, W. Nam, S. Fukuzumi, *Inorg. Chem. Front.* **2024**, *11*, 981.
[29] S. Fukuzumi, *Biochim. Biophys. Acta (BBA)-Bioenerg.* **2016**, *1857*, 604.
[30] E. R. Choban, L. J. Markoski, A. Wieckowski, P. J. Kenis, *J. Power Sources* **2004**, *128*, 54.
[31] R. Serra-Maia, M. Bellier, S. Chastka, K. Tranhuu, A. Subowo, J. D. Rimstidt, P. M. Usov, A. J. Morris, F. M. Michel, *ACS Appl. Mater. Interfaces* **2018**, *10*, 21224.
[32] B.-Q. Li, C.-X. Zhao, J.-N. Liu, Q. Zhang, *Adv. Mater.* **2019**, *31*, 1808173.
[33] A. Kulkarni, S. Siahrostami, A. Patel, J. K. Nørskov, *Chem. Rev.* **2018**, *118*, 2302.
[34] D. W. Flaherty, *ACS Catal.* **2018**, *8*, 1520.
[35] J. M. Campos-Martin, G. Blanco-Brieva, J. L. Fierro, *Angew. Chem.* **2006**, *118*, 7116.
[36] C. Xia, J. Y. Kim, H. Wang, *Nat. Catal.* **2020**, *3*, 605.
[37] Z. Zheng, Y. H. Ng, D.-W. Wang, R. Amal, *Adv. Mater.* **2016**, *28*, 9949.
[38] S. J. Freakley, Q. He, J. H. Harrhy, L. Lu, D. A. Crole, D. J. Morgan, E. N. Ntainjua, J. K. Edwards, A. F. Carley, A. Y. Borisevich, C. J. Kiely, G. J. Hutchings, *Science* **2016**, *351*, 965.
[39] J. K. Edwards, B. Solsona, A. F. Carley, A. A. Herzing, C. J. Kiely, G. J. Hutchings, *Science* **2009**, *323*, 1037.
[40] Q. Chang, P. Zhang, A. H. B. Mostaghimi, X. Zhao, S. R. Denny, J. H. Lee, H. Gao, Y. Zhang, H. L. Xin, S. Siahrostami, J. G. Chen Z. Chen, *Nat. Commun.* **2020**, *11*, 2178.
[41] Y. Miyase, S. Iguchi, Y. Miseki, T. Gunji, K. Sayama, *J. Electrochem. Soc.* **2019**, *166*, H644.
[42] E. Jung, H. Shin, B.-H. Lee, V. Efremov, S. Lee, H. S. Lee, J. Kim, W. Hooch Antink, S. Park, K.-S. Lee, S.-P. Cho, J. S. Yoo, Y.-E. Sung, T. Hyeon, *Nat. Mater.* **2020**, *19*, 436.
[43] Z. Wei, J. He, Y. Yang, Z. Xia, Y. Feng, J. Ma, *J. Energy Chem.* **2021**, *53*, 303.
[44] J. H. Montoya, L. C. Seitz, P. Chakthranont, A. Vojvodic, T. F. Jaramillo, J. K. Nørskov, *Nat. Mater.* **2017**, *16*, 70.
[45] P. Gallezot, *Chem. Soc. Rev.* **2012**, *41*, 1538.
[46] Y. Wen, T. Zhang, J. Wang, Z. Pan, T. Wang, H. Yamashita, X. Qian, Y. Zhao, *Angew. Chem.* **2022**, *134*, e202205972.
[47] K. Chan, J. K. Nørskov, *J. Phys. Chem. Lett.* **2015**, *6*, 2663.
[48] Z. Chen, S. Chen, S. Siahrostami, P. Chakthranont, C. Hahn, D. Nordlund, S. Dimosthenis, J. K. Nørskov, Z. Bao, T. F. Jaramillo, *React. Chem. Eng.* **2017**, *2*, 239.
[49] Y.-F. Han, Z. Zhong, K. Ramesh, F. Chen, L. Chen, T. White, Q. Tay, S. N. Yaakub, Z. Wang, *J. Phys. Chem. C* **2007**, *111*, 8410.
[50] S. Yang, Y. J. Tak, J. Kim, A. Soon, H. Lee, *ACS Catal.* **2017**, *7*, 1301.
[51] J. K. Edwards, S. J. Freakley, A. F. Carley, C. J. Kiely, G. J. Hutchings, *Acc. Chem. Res.* **2014**, *47*, 845.
[52] S. J. Freakley, M. Piccinini, J. K. Edwards, E. N. Ntainjua, J. A. Moulijn, G. J. Hutchings, *ACS Catal.* **2013**, *3*, 487.
[53] J. K. Edwards, J. Pritchard, L. Lu, M. Piccinini, G. Shaw, A. F. Carley, D. J. Morgan, C. J. Kiely, G. J. Hutchings, *Angew. Chem., Int. Ed.* **2014**, *53*, 2381.

[54] D. Kochubey, V. Chesnokov, S. Malykhin, *Carbon* **2012**, *50*, 2782.
[55] J. S. Jirkovsky, I. Panas, E. Ahlberg, M. Halasa, S. Romani, D. J. Schiffrin, *J. Am. Chem. Soc.* **2011**, *133*, 19432.
[56] S. Siahrostami, A. Verdaguer-Casadevall, M. Karamad, D. Deiana, P. Malacrida, B. Wickman, M. Escudero-Escribano, E. A. Paoli, R. Frydendal, T. W. Hansen, I. Chorkendorff, I. E. L. Stephens, J. Rossmeisl, *Nat. Mater.* **2013**, *12*, 1137.
[57] X. Hu, X. Zeng, Y. Liu, J. Lu, X. Zhang, *Nanoscale* **2020**, *12*, 16008.
[58] Y. Peng, B. Lu, S. Chen, *Adv. Mater.* **2018**, *30*, 1870370.
[59] H. Fei, J. Dong, D. Chen, T. Hu, X. Duan, I. Shakir, Y. Huang, X. Duan, *Chem. Soc. Rev.* **2019**, *48*, 5207.
[60] Z. Zhongming, L. Linong, Y. Xiaona, Z. Wangqiang, L. Wei, et al., *J. Am. Chem. Soc.* **2021**, *143*, 7819.
[61] H. Gong, Z. Wei, Z. Gong, J. Liu, G. Ye, M. Yan, J. Dong, C. Allen, J. Liu, K. Huang, R. Liu, G. He, S. Zhao, H. Fei, *Adv. Funct. Mater.* **2022**, *32*, 2106886.
[62] E. Jung, H. Shin, W. H. Antink, Y. Sung, *ACS Energy Lett.* **2020**, *5*, 1881.
[63] K. Huang, Z. Wei, J. Liu, Z. Gong, J. Liu, M. Yan, G. He, H. Gong, Y. Hu, Y. He, S. Zhao, G. Ye, H. Fei, *Small* **2022**, *18*, 2201139.
[64] S. Yang, A. Verdaguer-Casadevall, L. Arnarson, L. Silvioli, V. Colic, R. Frydendal, J. Rossmeisl, I. Chorkendorff, I. E. Stephens, *ACS Catal.* **2018**, *8*, 4064.
[65] C. Xia, S. Back, S. Ringe, K. Jiang, F. Chen, X. Sun, S. Siahrostami, K. Chan, H. Wang, *Nat. Catal.* **2020**, *3*, 125.
[66] W. Li, A. Bonakdarpour, E. Gyenge, D. P. Wilkinson, *ChemSusChem* **2013**, *6*, 2137.
[67] J.-D. Xiao, H.-L. Jiang, *Acc. Chem. Res.* **2018**, *52*, 356.
[68] R. Ferrigno, A. D. Stroock, T. D. Clark, M. Mayer, G. M. Whitesides, *J. Am. Chem. Soc.* **2002**, *124*, 12930.
[69] R. S. Jayashree, L. Gancs, E. R. Choban, A. Primak, D. Natarajan, L. J. Markoski, P. J. Kenis, *J. Am. Chem. Soc.* **2005**, *127*, 16758.
[70] C. Zhao, S. Yuan, X. Cheng, Z. Zheng, J. Liu, J. Yin, S. Shen, X. Yan, J. Zhang, *Energy and AI* **2023**, *13*, 100245.
[71] H. Wang, Z. Xu, W. Lin, X. Yang, X. Gu, W. Zhu, Z. Zhuang, *Nano Res.* **2023**, *16*, 420.
[72] Y. J. Kim, A. Lim, J. M. Kim, D. Lim, K. H. Chae, E. N. Cho, H. J. Han, K. U. Jeon, M. Kim, G. H. Lee, H. S. Ahn, H. S. Park, H. Kim, J. Y. Kim, Y. S. Jung, *Nat. Commun.* **2020**, *11*, 4921.
[73] Y. Zhang, Y. Lin, R. Li, Z. Chen, D. Zeng, S. Chen, W. Wang, L. Zhang, W. Wang, H. Nie, G. Wang, *Chem. Eng. J.* **2023**, *465*, 143043.
[74] G. Korotcenkov, B. Cho, L. Gulina, V. Tolstoy, *J. Teknol.* **2015**, *75*, 15.
[75] L. B. Gulina, V. P. Tolstoy, A. A. Solovev, V. E. Gurenko, G. Huang, Y. Mei, *Prog. Nat. Sci.: Mater. Int.* **2020**, *30*, 279.
[76] K. Hyun, S. Kang, J. Kim, Y. Kwon, *ACS Appl. Mater. Interfaces* **2020**, *12*, 23635.
[77] V. Briega-Martos, E. Herrero, J. M. Feliu, *Electrochim. Acta* **2020**, *334*, 135452.
[78] K. N. da Silva, R. Nagao, E. Sitta, *ChemistrySelect* **2017**, *2*, 11713.
[79] C. Dehchar, I. Chikouche, A. Hamam, A. Zouaoui, A. Sahari, F. Deflorian, S. Belfar, *Inorg. Chem. Commun.* **2020**, *116*, 107905.
[80] S. Strbac, *Electrochim. Acta* **2011**, *56*, 1597.
[81] F. Yang, K. Cheng, X. Liu, S. Chang, J. Yin, C. Du, L. Du, G. Wang, D. Cao, *J. Power Sources* **2012**, *217*, 569.
[82] R. Rizo, J. M. Feliu, E. Herrero, *J. Catal.* **2021**, *398*, 123.
[83] D. Cao, J. Chao, L. Sun, G. Wang, *J. Power Sources* **2008**, *179*, 87.
[84] N. C. D. Nath, T. Debnath, E.-K. Kim, M. A. A. Shaikh, J.-J. Lee, *Electrochim. Acta* **2018**, *273*, 474.
[85] S. J. Amirfakhri, J.-L. Meunier, D. Berk, *J. Power Sources* **2014**, *272*, 248.
[86] D. Cardoso, B. Šljukić, N. Sousa, C. Sequeira, F. Figueiredo, D. Santos, *Phys. Chem. Chem. Phys.* **2018**, *20*, 19045.
[87] Y. Xue, W. Cai, S. Zheng, W. Yan, J. Hu, Z. Sun, Y. Zhang, W. Jin, *Catal. Sci. Technol.* **2017**, *7*, 5733.
[88] S. J. Amirfakhri, D. Binny, J.-L. Meunier, D. Berk, *J. Power Sources* **2014**, *257*, 356.
[89] S.-Y. Hsu, C.-L. Lee, C.-H. Kuo, W.-C. Kuo, *Sens. Actuators, B* **2021**, *328*, 129015.
[90] Z. Li, Y. He, X. Ke, L. Gan, J. Zhao, G. Cui, G. Wu, *J. Power Sources* **2015**, *294*, 136.
[91] R. Mažeikienė, G. Niaura, A. Malinauskas, *J. Electroanal. Chem.* **2011**, *660*, 140.
[92] X. Xiao, F. Yang, K. Cheng, X. Wang, H. Zhang, K. Ye, G. Wang, D. Cao, *Int. J. Hydrogen Energy* **2017**, *42*, 22856.
[93] R. Martins, D. Martins, L. Costa, T. Matencio, R. Paniago, L. Montoro, *Int. J. Hydrogen Energy* **2020**, *45*, 25708.
[94] K. Muñoz-Becerra, D. F. Báez, J. H. Zagal, S. Bollo, A. Toro-Labbé, R. Venegas, F. J. Recio, *Electrochim. Acta* **2020**, *357*, 136881.
[95] S. Eugénio, D. Cardoso, D. Santos, B. Šljukić, M. Montemor, *Int. J. Hydrogen Energy* **2016**, *41*, 14370.
[96] Y. Zhang, Y. Zhao, S. Shi, M. Tian, H. Yin, *Ionics* **2018**, *24*, 1457.
[97] S. N. Faisal, E. Haque, N. Noorbehesht, H. Liu, M. M. Islam, L. Shabnam, A. K. Roy, E. Pourazadi, M. S. Islam, A. T. Harris, et al., *Sustainable Energy Fuels* **2018**, *2*, 2081.
[98] J. Ji, Y. Chung, Y. Kwon, *J. Power Sources* **2020**, *480*, 228860.
[99] J. Ji, K. Im, H. An, S. J. Yoo, Y. Chung, J. Kim, Y. Kwon, *Int. J. Energy Res.* **2022**, *46*, 760.
[100] M. Piescheck, A. Abdelrahman, J. M. Hermann, H. Müller, T. Jacob, L. A. Kibler, *Electrocatalysis* **2021**, *12*, 264.
[101] J. Ji, Y. Chung, Y. Kwon, *J. Mater. Chem. C* **2020**, *8*, 2749.
[102] X. Wang, K. Ye, H. Zhang, X. Ma, K. Zhu, K. Cheng, G. Wang, D. Cao, *Int. J. Hydrogen Energy* **2017**, *42*, 15044.
[103] T. H. Lee, S. S. Yu, T. H. Oh, *Int. J. Hydrogen Energy* **2023**, *48*, 18845.
[104] R. Raman, S. Prashant, A. Shukla, *J. Power Sources* **2006**, *162*, 1073.
[105] R. O. Stroman, G. S. Jackson, Y. Garsany, K. Swider-Lyons, *J. Power Sources* **2014**, *271*, 421.
[106] M. Abdolmaleki, M. Hosseini, *Fuel Cells* **2017**, *17*, 321.
[107] G. Selvarani, S. Prashant, A. Sahu, P. Sridhar, S. Pitchumani, A. Shukla, *J. Power Sources* **2008**, *178*, 86.
[108] C. P. de León, F. Walsh, C. Patrissi, M. Medeiros, R. Bessette, R. Reeve, J. Lakeman, A. Rose, D. Browning, *Electrochem. Commun.* **2008**, *10*, 1610.
[109] B. Li, C. Song, X. Huang, K. Ye, K. Cheng, K. Zhu, J. Yan, D. Cao, G. Wang, *ACS Sustainable Chem. Eng.* **2019**, *7*, 11129.
[110] L. An, T. Zhao, R. Chen, Q. Wu, *J. Power Sources* **2011**, *196*, 6219.
[111] A. E. Sanli, M. Gordesel, E. S. Yilmaz, S. K. Ozden, G. Gunlu, B. Z. Uysal, *Int. J. Hydrogen Energy* **2017**, *42*, 8119.
[112] Y. Ko, J. Park, X. Zhang, L. Kang, T. H. M. Pham, V. Boureau, C. Pham-Huu, J. Kim, L. Zhong, A. Züttel, *ChemRxiv* **2023, 1, 1**.
[113] W. Haijun, W. Cheng, L. Zhixiang, M. Zongqiang, *Int. J. Hydrogen Energy* **2010**, *35*, 2648.
[114] G. Agladze, P. Nikoleishvili, V. Kveselava, G. Tsurtsumia, G. Gorelishvili, D. Gogoli, I. Kakhniashvili, *J. Power Sources* **2012**, *218*, 46.
[115] R. M. E. Hjelm, Y. Garsany, R. W. Atkinson, R. O. Stroman, K. Swider-Lyons, C. Lafforgue, M. Chatenet, *ECS Trans.* **2017**, *80*, 1033.
[116] W. Sangarunlert, S. Sukchai, A. Pongtornkulpanich, A. Nathakaranakule, T. Luschtinetz, *J. Fuel Cell Sci. Technol.* **2011, *8*, 061**.
[117] O. Hasvold, K. H. Johansen, in *Proceedings of the 2002 Workshop on Autonomous Underwater Vehicles, 2002*, IEEE, Piscataway **2002**, pp. 89–94.
[118] L. Yi, B. Hu, Y. Song, X. Wang, G. Zou, W. Yi, *J. Power Sources* **2011**, *196*, 9924.
[119] K. Naga Mahesh, R. Balaji, K. Dhathathreyan, *Ionics* **2015**, *21*, 2603.

[120] L. Yi, Y. Song, W. Yi, X. Wang, H. Wang, P. He, B. Hu, *Int. J. Hydrogen Energy* **2011**, *36*, 11512.
[121] L. Yi, L. Liu, X. Wang, X. Liu, W. Yi, X. Wang, *J. Power Sources* **2013**, *224*, 6.
[122] J. Wei, X. Wang, Y. Wang, J. Guo, P. He, S. Yang, N. Li, F. Pei, Y. Wang, *Energy Fuels* **2009**, *23*, 4037.
[123] L. Yi, B. Yu, W. Yi, Y. Zhou, R. Ding, X. Wang, *ACS Sustainable Chem. Eng.* **2018**, *6*, 8142.
[124] L. Yi, Y. Hu, J. Fei, J. Li, C. Yang, X. Wang, *J. Solid State Electrochem.* **2019**, *23*, 1739.
[125] L. Yi, L. Liu, X. Liu, X. Wang, W. Yi, P. He, X. Wang, *Int. J. Hydrogen Energy* **2012**, *37*, 12650.
[126] R. Venkatachalapathy, G. P. Davila, J. Prakash, *Electrochem. Commun.* **1999**, *1*, 614.
[127] Y. H. Hong, Y.-M. Lee, W. Nam, S. Fukuzumi, *J. Porphyrins Phthalocyanines* **2023**, *27*, 11.
[128] R. Zeis, T. Lei, K. Sieradzki, J. Snyder, J. Erlebacher, *J. Catal.* **2008**, *253*, 132.
[129] N. A. Savastenko, K. Anklam, A. Quade, M. Brüser, A. Schmuhl, V. Brüser, *Energy Environ. Sci.* **2011**, *4*, 3461.
[130] X. Yan, F. Meng, Y. Xie, J. Liu, Y. Ding, *Sci. Rep.* **2012**, *2*, 941.
[131] B. Li, C. Song, J. Yin, J. Yan, K. Ye, K. Cheng, D. Cao, G. Wang, *Int. J. Hydrogen Energy* **2020**, *45*, 10569.
[132] K. Hayashi, T. Tomimori, R. Sato, N. Todoroki, T. Wadayama, *Phys. Chem. Chem. Phys.* **2023**, *25*, 2770.
[133] M. Hosseini, R. Mahmoodi, *J. Power Sources* **2017**, *370*, 87.
[134] C. Yunphuttha, S. Porntheeraphat, S. Midpanon, A. Wongchaisuwat, P. Viravathana, *J. Power Sources* **2018**, *392*, 251.
[135] H. Meng, M. Wu, X. Hu, M. Nie, Z. Wei, P. Shen, *Fuel Cells* **2006**, *6*, 447.
[136] J. Tang, T. Zhao, D. Solanki, X. Miao, W. Zhou, S. Hu, *Joule* **2021**, *5*, 1432.
[137] K. Fujiwara, A. Akita, S. Kawano, M. Fujishima, H. Tada, *Electrochem. Commun.* **2017**, *84*, 71.
[138] C. Song, D. Zhang, K. Ye, W. Zeng, X. Yang, Y. Wang, Y. Shen, D. Cao, K. Cheng, G. Wang, *J. Electroanal. Chem.* **2017**, *788*, 74.
[139] J. Liu, L. Yi, X. Wang, Q. Zhao, Y. Zhang, J. Gao, W. Wei, *Int. J. Hydrogen Energy* **2015**, *40*, 7301.
[140] H. Wang, Y. Wang, X. Wang, P. He, L. Yi, W. Yi, X. Liu, et al., *Int. J. Electrochem.* **2011**, *2011*, 1.
[141] M. G. Hosseini, V. Daneshvari-Esfahlan, H. Aghajani, S. Wolf, V. Hacker, *Catalysts* **2021**, *11*, 1372.
[142] T. S. Andrade, B. A. C. Sá, I. C. Sena, A. R. S. Neto, F. G. E. Nogueira, P. Lianos, M. C. Pereira, *J. Electroanal. Chem.* **2021**, *881*, 114948.
[143] A. E. Sanlı, *Int. J. Energy Res.* **2013**, *37*, 1488.
[144] P. S. Khadke, P. Sethuraman, P. Kandasamy, S. Parthasarathi, A. K. Shukla, *Energies* **2009**, *2*, 190.
[145] J. Peng, Z. Zhang, H. Niu, *Fuel Cells* **2012**, *12*, 1009.
[146] Y. Yang, Y. Xue, F. Huang, H. Zhang, K. Tao, R. Zhang, Q. Shen, H. Chang, *ACS Appl. Energy Mater.* **2018**, *1*, 5328.
[147] S. Wang, D. Ye, Z. Liu, X. Zhu, R. Chen, Q. Liao, Y. Yang, H. Liu, *Int. J. Hydrogen Energy* **2022**, *47*, 4793.
[148] A. Li, S. H. Chan, N.-T. Nguyen, *J. Micromech. Microeng.* **2007**, *17*, 1107.
[149] I. Chino, O. Muneeb, E. Do, V. Ho, J. L. Haan, *J. Power Sources* **2018**, *396*, 710.
[150] X. Yan, A. Xu, L. Zeng, P. Gao, T. Zhao, *Energy Techn.* **2018**, *6*, 140.
[151] M. Tanveer, E. S. Lim, K.-Y. Kim, *Fuel* **2021**, *298*, 120818.
[152] A. E. Sanli, M. L. Aksu, B. Z. Uysal, *Int. J. Hydrogen Energy* **2011**, *36*, 8542.
[153] M. Çelik, *Turkish J. Eng.* **2022**, *6*, 161.
[154] F. Chen, M.-H. Chang, C.-W. Hsu, *Electrochim. Acta* **2007**, *52*, 7270.
[155] S. M. M. Ehteshami, M. Asadnia, S. N. Tan, S. H. Chan, *J. Power Sources* **2016**, *301*, 392.
[156] J.-C. Shyu, C.-L. Huang, *J. Power Sources* **2011**, *196*, 3233.
[157] A. Yang, J. Tseng, C. Wen, H. Zhang, *J. Electrochem. Energy Conv. Storage* **2020**, *17*, 031009.
[158] J.-C. Shyu, C.-L. Huang, T.-S. Sheu, H. Ay, *Micro Nano Lett.* **2012**, *7*, 740.
[159] Y. Yang, Y. Xue, H. Zhang, H. Chang, *Chem. Eng. J.* **2019**, *369*, 813.
[160] J.-C. Shyu, C.-S. Wei, C.-J. Lee, C.-C. Wang, *Appl. Therm. Eng.* **2010**, *30*, 1863.
[161] Z. Liu, D. Ye, S. Wang, X. Zhu, R. Chen, Q. Liao, *Ind. Eng. Chem. Res.* **2020**, *59*, 15447.
[162] E. Kjeang, R. Michel, D. A. Harrington, N. Djilali, D. Sinton, *J. Am. Chem. Soc.* **2008**, *130*, 4000.
[163] L.-L. Zhang, S. Duan, X.-L. Yang, G. Liang, Y.-H. Huang, X.-Z. Cao, J. Yang, M. Li, M. C. Croft, C. Lewis, *J. Power Sources* **2015**, *278*, 826.
[164] M. Nasharudin, S. Kamarudin, U. Hasran, M. Masdar, *Int. J. Hydrogen Energy* **2014**, *39*, 1039.
[165] M.-A. Goulet, E. Kjeang, *Electrochim. Acta* **2014**, *140*, 217.
[166] G. L. Soloveichik, *Beilstein J. Nanotechnol.* **2014**, *5*, 1399.
[167] E. H. Yu, X. Wang, U. Krewer, L. Li, K. Scott, *Energy Environ. Sci.* **2012**, *5*, 5668.
[168] F. Sharifi, S. Ghobadian, F. R. Cavalcanti, N. Hashemi, *Renewable Sustainable Energy Rev.* **2015**, *52*, 1453.
[169] L.-L. Shen, G.-R. Zhang, B. J. Etzold, *ChemElectroChem* **2020**, *7*, 10.
[170] J. C. Kurnia, B. A. Chaedir, A. P. Sasmito, T. Shamim, *Appl. Energy* **2021**, *283*, 116359.
[171] M. K. Rashed, M. A. Mohd Salleh, H. A. Abdulbari, M. H. Shah Ismail, S. Izhar, *ChemBioEng Rev.* **2015**, *2*, 356.
[172] I. Hanapi, S. Kamarudin, A. Zainoodin, U. Hasran, *Int. J. Energy Res.* **2019**, *43*, 8956.
[173] Q. Lan, D. Ye, X. Zhu, R. Chen, Q. Liao, T. Zhang, Y. Zhou, *ACS Sustainable Chem. Eng.* **2021**, *9*, 5623.
[174] C. Liu, L. Liu, X. Wang, B. Xu, W. Lan, *Ind. Eng. Chem. Res.* **2018**, *57*, 13557.
[175] R. Wu, D. Ye, R. Chen, B. Zhang, X. Zhu, H. Guo, Z. Liu, *Int. J. Energy Res.* **2020**, *44*, 2243.
[176] Y. Zhou, B. Zhang, X. Zhu, D.-D. Ye, R. Chen, T. Zhang, X.-L. Gong, Q. Liao, *J. Power Sources* **2020**, *445*, 227326.
[177] A. Jindal, S. Basu, N. Chauhan, T. Ukai, D. S. Kumar, K. Samudhyatha, *J. Power Sources* **2017**, *342*, 165.
[178] O. Muneeb, I. Chino, A. Saenz, J. L. Haan, *J. Power Sources* **2019**, *413*, 216.
[179] C. A. Campos-Roldan, H. Zhong, S. M. Unni, R. d. G. Gonzalez-Huerta, Y. Feng, N. Alonso-Vante, *ACS Appl. Energy Mater.* **2020**, *3*, 7397.
[180] S. Hasegawa, K. Shimotani, K. Kishi, H. Watanabe, *Electrochem. Solid-State Lett.* **2004**, *8*, A119.
[181] T. S. Copenhaver, K. H. Purohit, K. Domalaon, L. Pham, B. J. Burgess, N. Manorothkul, V. Galvan, S. Sotez, F. A. Gomez, J. L. Haan, *Electrophoresis* **2015**, *36*, 1825.
[182] V. Galvan, K. Domalaon, C. Tang, S. Sotez, A. Mendez, M. Jalali-Heravi, K. Purohit, L. Pham, J. Haan, F. A. Gomez, *Electrophoresis* **2016**, *37*, 504.
[183] Y. Li, W. Van Roy, P. M. Vereecken, L. Lagae, *Microelectron. Eng.* **2017**, *181*, 47.

[184] A. Kar, T.-Y. Chiang, I. Ortiz Rivera, A. Sen, D. Velegol, *ACS Nano* **2015**, *9*, 746.
[185] L. Hu, N. Wang, K. Tao, in *Smart nanosystems for biomedicine, optoelectronics and catalysis*, IntechOpen, Rijeka **2020**.
[186] A. A. Solovev, *Catalytic Tubular Micro-Jet Engines*, MONARCH Online Database **2012**.
[187] S. Naeem, F. Naeem, M. Manjare, F. Liao, V. Bolaños Quiñones, G. Huang, Y. Li, J. Zhang, A. Solovev, Y. Mei, *Appl. Phys. Lett.* **2019**, *114*, 033701.

**Aleksei Kuzin** has obtained B.Sc. degree with honors in Infocommunication Technologies and Systems from National Research University Higher School of Economics (MIEM) in 2019. He has obtained master's degree with honors from the Skolkovo Institute of Science and Technology in 2021 in the field of Photonics and Quantum Materials. Currently, Aleksei is a third-year Ph.D. student in the Skolkovo Institute of Science and Technology. His research interests are related to combination of photonic integrated circuits and acoustic tweezer technologies on microfluidic channels for biomedicine applications.

**Mr. Fenyang Zhu** received his B.D. in College of Materials Science and Engineering at Donghua University in 2022, Shanghai. After that, he joined in Nanomembrane group as master student in the department of material science at Fudan University, Shanghai. At present, he is working on his master degree in the field of one-compartment hydrogen peroxide fuel cells and electromagnetical manipulation of microbots.

**Prof. Gaoshan Huang** received his Ph.D. in condensed mater physics at Nanjing University, China in 2007. After graduation, he worked in IFW Dresden, Germany as a guest scientist. Then he moved to IMRE, Singapore as a research engineer. In 2010, he joined the Department of Materials Science, Fudan University, China. Currently, he is a professor of materials science at Fudan University. His research interest is fabrications and characterizations of low-dimensional structures.

**Professor Alexander A. Solovev** www.solovevlab.comreceived his Ph.D. from the Leibniz Institute for Solid State and Materials Research, Dresden Germany. As one of the founders of man-made nanomachines field, he was a visiting scholar at Harvard University and held a full professorship at Fudan University, where his group achieved breakthroughs in inorganic nanomembranes, yielding novel quantum, chemical, electrical, optical, and mechanical properties. His accolades include the IOP Science Emerging Leader Award, the Australian Global Talent, the Chinese "1000 Talent" Award, the Humboldt Feodor Lynen Fellowship, Max Planck Fellowship and the Guinness World Record for the smallest man-made jet engine. His research encompasses strain-engineered nanomaterials, nano/micromachines, microfluidics for clean energy, biomedicine, and environmental sustainability.